university of groningen / faculty of science and engineering

Using CFD analysis to investigate noise reduction on a wind turbine blade

Master Research Project

Industrial Engineering and Management

Author:
Kate Schoen — S4477111

Supervisors:
ir. P.D. (Pablo) Druetta, Dr
D. (Daniele) Parisi, PhD

21st of March 2025

Acknowledgments

I would like to thank everyone who helped me throughout this project. First and foremost, I would like to express my gratitude to my supervisor, Pablo, for his guidance throughout this project. He never turned me away when I had questions, especially in my endless troubles with COMSOL at the beginning. I also thank my second supervisor, Daniele, for his input and support along the way, as well as the occasional padel match. I would like to thank Enrique, who went above and beyond to help me with the flow tank configurations. Finally, I want to extend my appreciation to my office mates: Ana, Marijn, Pradito, Ralph, Simon, Amanda, Kees, Giorgio, and Marco for their company and support in this project.

Abstract

Wind turbine noise remains a significant barrier to the expansion of onshore wind energy, as noise regulations and irritations limit the placement of turbines near residential areas. This research investigates aerodynamic noise reduction strategies through Computational Fluid Dynamics simulations using the RANS - Shear Stress Transport turbulence model in COMSOL Multiphysics®. The study focuses on reducing noise by investigating different combinations of parameters, namely; the blade shape, angle of attack, wind direction, and surface roughness. This noise reduction is first investigated by measuring the Turbulence Kinetic Energy, a key factor in noise generation. Subsequently, the dBA is interpreted from the CFD data in MATLAB to make a direct comparison in terms of sound. The parameters were tested in different combinations, with a heavier focus falling on the three selected blade shapes of: an improved shape, a geometric fin addition, and the addition of serrations. Results indicate that serrations on the trailing edge effectively disrupt vortex shedding, leading to a measurable reduction in Sound Pressure Level. This could further be improved by also reducing the number of serrations at the very tip of the blade in order to not interact with the tip vortex formation. In addition, the improved basic shape with less rotation also shares the same promising results. The simulations showed that a reduction of 3 dBA was achievable with both the serrated design as well as the improved basic shape. These conclusions were also achieved when the samples were tested using a flow tank with a Reynold's number similar to the computational studies. To further improve the accuracy of the models, it is recommended to simulate using time-dependent studies that use LES modeling to enhance turbulence resolution. Finally, refining the way the blade rugosity is modeled would be a useful study to better understand and analyze how coatings could be used to reduce noise.

Abbreviations

AoA - Angle of Attack

CAD - Computer Aided Design

CFD - Computational Fluid Dynamics

COMSOL - COMSOL Multiphysics ®

dBA - A-weighted decibel

FPS - Frames Per Second

FW-H - Ffowcs Williams-Hawkings

LBL - Laminar Boundary Layer

NACA - National Advisory Committee for Aeronautics

N-S - Navier-Stokes

PIV - Particle Image Velocimetry

RANS - Reynolds-Averaging Navier Stokes

RPM - Revolutions Per Minute

SPL - Sound Pressure Level

SST - Shear Stress Transport

TBL - Turbulent Boundary Layer

TE - Trailing Edge

TKE - Turbulent Kinetic Energy

VS - Vortex Shedding

Contents

1 Introduction

The Netherlands is moving toward a more sustainable future in terms of energy. One of their key focuses with this movement is wind energy given their position on the coast and the lack of high solar insolation throughout the year [1]. The Netherlands' use of wind energy spans back centuries from early grain windmills to now producing thousands of wind turbines to keep up with these growing renewable energy demands. By the end of 2020, the country had a total of 2606 wind turbines, with 2144 of these being placed on shore [2]. The government aims for wind energy to be the largest source of electricity in the country by 2030 [1], with these expansion goals, cost and space constraints are naturally the largest hindrance towards achieving this goal. The cost of a wind turbine usually pays itself back 6 months after the operation begins [3], with the efficiency of the turbine sitting around 20% at its lowest and 40% at its peak depending on the wind [4].

One of the primary hindrances of these current problems is the noise produced by wind turbines [5; 6; 7]. With varying regulations in place for how much noise turbines can produce, any noise reduction to the design that can offer up to a dBA is highly needed to obtain optimal energy production from the turbines [8]. Noise trade-offs can include operating at reduced speeds or with modified pitch angles to minimize sound emissions [9]. This is demonstrated in Figure 1 [8], where the standard setting can be reduced in power to achieve a lower noise output. This is the current state-of-the-art in wind turbine design with respect to noise. However, these approaches can significantly impact the economic viability of wind energy projects. With the growing number of turbines and the increasing need for energy, more importance is placed understanding and reducing this noise [9]. If the standard setting can be operated with 5 dB less noise, this means more energy per turbine [8].

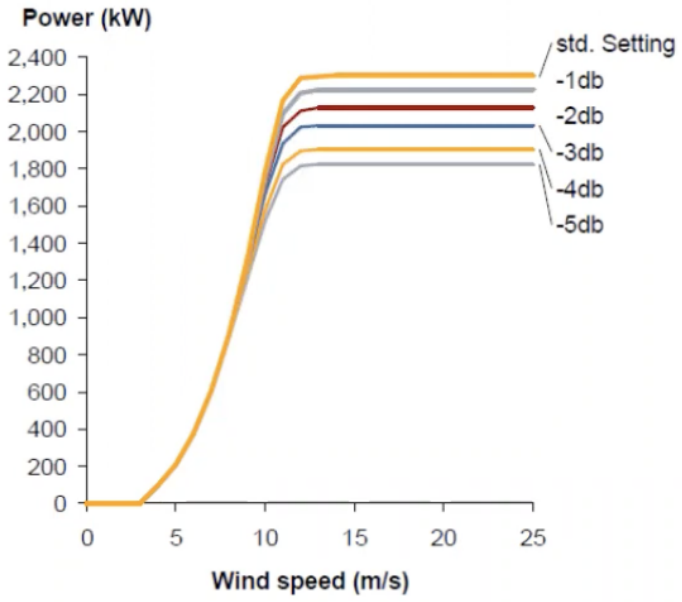

Figure 1: The power produced by a wind turbine under different operation settings. The sacrifice of noise shows a proportional reduction in power. Taken from [8].

The current state-of-the-art in solving this issue turns to geometric designs that could help reduce the turbulence. This research tends to focus on disruptive designs that alter vortex shapes. This research rarely investigates the overlapping factors that can affect this noise

reduction. In this research project, an approach to reduce the noise produced by wind turbines will be found. In addition, different factors which influence the noise reduction will also be investigated. This will be executed by first analyzing the problem and solving it numerically and subsequently testing the designs in a flow tank.

2 Problem Analysis

There are two ways to discuss the issue of limited space for wind turbines. The first approach is whether there is sufficient area to put wind turbines such that they are not going to interfere with the efficiency of other surrounding turbines [10]. Placing turbines too close to each other's proximity means that the turbulence from their interaction with the wind decreases the efficiency of the next turbine, resulting in suboptimal energy harvesting [10]. The second problem with space is finding locations far enough from populated areas due to the noise of the turbines. Populated areas near wind turbines often complain about the noise and visual impact of wind turbines on their communities. In addition, several long-term health impacts have also been sourced as a problem [11]. Increasing the number of offshore wind turbines has also become a very limited approach to this problem. Although noise is not a problem offshore, there are limited amounts of turbines that can be placed without the need to support them very deep underwater. Support underwater is expected to an extent, but can quickly lead to high costs when placed in water deeper than 30 meters [12]. In addition, there are other limitations to offshore wind turbines. Transportation and storage of their energy have much higher costs than for turbines onshore [12]. Therefore, addressing the noise produced by wind turbines is a tool that can be used to keep up with the increasing energy demand onshore [9].

Noise pollution is a major concern that directly relates to their design. Several rules have been put in place about the distance a wind turbine can be to people due to their noise production [9]. Noise is measured on a logarithmic scale in dB or dBA. dBA are A-weighted decibels, which adjust decibels for human hearing sensitivity by emphasizing mid-level frequencies and reducing very low and high frequencies, while dB is a general measure of sound intensity without frequency weighting. The logarithmic scale of the measurement makes any small adjustment already impactful. Current acceptable noise levels go up to 55 dBA during the daytime, however, these levels are already classified as a "serious annoyance". During the night, acceptable noise levels are reduced to 40 dBA to avoid sleep disturbance. 40 dBA can be compared to the noise from a loud refrigerator, typical background noise, whereas 55 dBA is the level of noise expected from a conversation [13]. Typical wind turbine noise is around 35 to 45 dBA from 300 meters away [14]. In The Netherlands, turbines are permitted to be 400 meters away from the nearest house [15]. This distance is already much shorter than other countries such as Germany and Belgium whose values are more than 800 meters from the nearest residential houses [15]. This applies to wind turbines with a higher power output, producing energy at a capacity of more than 2 MW [16].

Although substantial efforts have been made to mitigate this issue, the increasing size of wind farms and limited applicability in placing them close to each other result in the turn toward noise reduction as a potential solution to place more turbines on shore.

2.1 Problem Context

This problem has existed for decades during the scaling up of wind turbines as an energy source [9]. It remains a problem due to the trade-offs that exist in solving it. The best shape for noise does not necessarily harvest as much energy. Wind turbines, in their purest essence, harvest the energy from the wind through the kinetic energy from the wind moving the turbine blades. This is highly dependent on the speed of the wind naturally, but is also very relevant to the amount of lift created by the wind. The shape and positioning of the blade help create more lift than drag, which in turn helps the blades rotate quicker and thus have more kinetic energy [17]. Because the goal of turbines is to produce the most energy, often efficiency and creating the most lift are prioritized in the design stage, rather than noise [18]. Solving this problem therefore involves searching for a trade-off between noise and efficiency.

There are two main types of noise generated by wind turbines: aerodynamic and mechanical [19]. Mechanical noise is a result of the inner workings of the turbine, and the loudest components are often the gear train and turbines. However, these are consistent noise patterns and are regularly improved by designing these components in the turbine. In addition, they are within a casing as part of the wind turbine, which permits there to be some more sound isolation The larger problem lies in the aerodynamic noise produced by the wind turbines. Aerodynamic noise is caused by the interaction of the wind with the blades, which tends to be the more prominent and bothersome issue given the inconsistency [19].

The aerodynamic noise stems from air interacting with a solid, resulting in disturbance of the fluid and its flow pattern [19]. This type of fluid dynamics is always governed by the Navier-Stokes equation, which is used to describe the movement in fluids [20][21]. The Navier-Stokes equation is also accompanied by the continuity equation, which abides by the conservation of mass in the fluid. The NS equation of motion describes the behavior of the fluid velocity over time through impact from viscosity, pressure and external forces (such as gravity). What is first relevant to differentiate is that the flow is incompressible [20]. This can be differentiated, as the wind velocity for turbine operation does not exceed 30 m/s. As a result, the Mach number will never exceed 0.1, permitting the assumption that the air flow is incompressible. The governing Navier-Stokes equation is equation 1, with the stress tensor τ further expanded in equation 2, for an incompressible flow. The continuity equation is shown in equation 3, which is the viscous stress tensor [21].

$$\frac{\partial(\rho\mathbf{u})}{\partial t} + \nabla \cdot (\rho\mathbf{u} \otimes \mathbf{u}) = -\nabla p + \nabla \cdot \boldsymbol{\tau} + \rho\mathbf{f} \tag{1}$$

$$\boldsymbol{\tau} = \mu \left(\nabla\mathbf{u} + (\nabla\mathbf{u})^T\right) \tag{2}$$

$$\frac{\partial\rho}{\partial t} + \nabla \cdot (\rho\mathbf{u}) = 0 \tag{3}$$

These equations govern the fluid flow and hence the way the flow creates aerodynamic noise. There are five different types of aerodynamic noise. These are turbulent boundary layer trailing edge (TBL-TE) noise, separation stall noise, laminar boundary layer vortex shedding (LBL-VS) noise, trailing edge bluntness vortex shedding (TEB-VS) noise and turbulent inflow noise [19]. These can be categorized to simplify where they are coming from and what effects they have on the flow pattern. The most prevalent noise is that produced by the trailing edge of the blade (see Figure 2), relating to TBL-TE and TEB-VS [19; 22]. The majority of the turbine blade is uniform in shape and therefore produces the same amount of noise along this trailing edge [22]. The leading edge noise comes from the separation stall noise, or turbulent

inflow noise and is responsible for the majority of LBL-VS noise [22]. The next distinction comes from defining turbulent flow, laminar flow and vortex shedding as it relates to the noise categories.

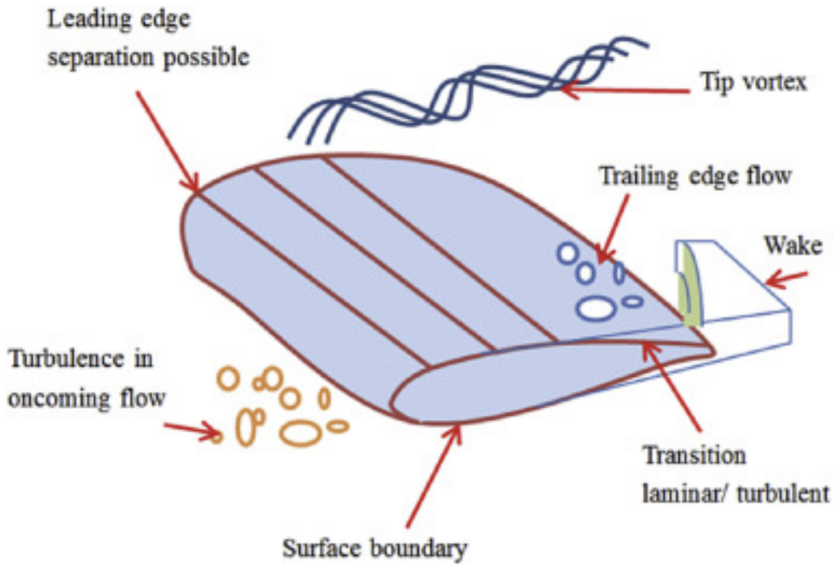

Figure 2: Different flow patterns over a wind turbine airfoil, taken from [19].

Turbulent and laminar flow relate to another key principle that governs fluid dynamics. This is the Reynold's number of a fluid. The Reynold's number is defined as [21]:

$$Re = \frac{\rho v D}{\mu} \tag{4}$$

This relation looks at a fluid's velocity, density, viscosity and its length/diameter in order to define whether the fluid is behaving very orderly and 'smooth', also referred to as laminar, or whether the fluid is behaving more erratic [21]. A low Reynolds number indicates that viscous forces dominate, leading to laminar flow. In contrast, a high Reynolds number means that inertial forces dominate, causing turbulent flow. In Figure 3 [23], the difference between these two types of flow is shown visually. Within turbulent flow, vortices are formed, which are eddies that arise in the fluid and contribute to the energy dissipation characteristic of turbulence.

The formation of vortices contributes to vortex shedding [19]. This is the additional formation of vortices downstream from the body with which the fluid interacts. The separation of the fluid from the boundary layer creates vortices due to the differences in pressure, which results in circular flow patterns due to high and low pressure coming from opposing sides of the blade [23; 22]. These naturally increase with more turbulent flow as there is more separation. Provided that this separation does not change significantly, the oscillations of the vortices may remain fairly constant. But this simply results in a constant noise. Vibrations within the solid structure are also a frequent consequence of the vortices along with the noise formation [19].

One of the primary sources of the noise is the blade tip, the reduction in size is responsible for higher vortex formation, which produces more noise. In addition, the blade ending also produces a tip vortex. This is a product of trailing edge bluntness vortex shedding noise [19]. The wind speed is higher at the tip of the blade due to the centrifugal forces. The

higher speed causes a greater formation of eddies, and as a result vortices. The interaction of this turbulence with the solid materials causes there to be noise in addition to only the aerodynamic noise. This is an additional source of low frequency noise that causes disturbance [14].

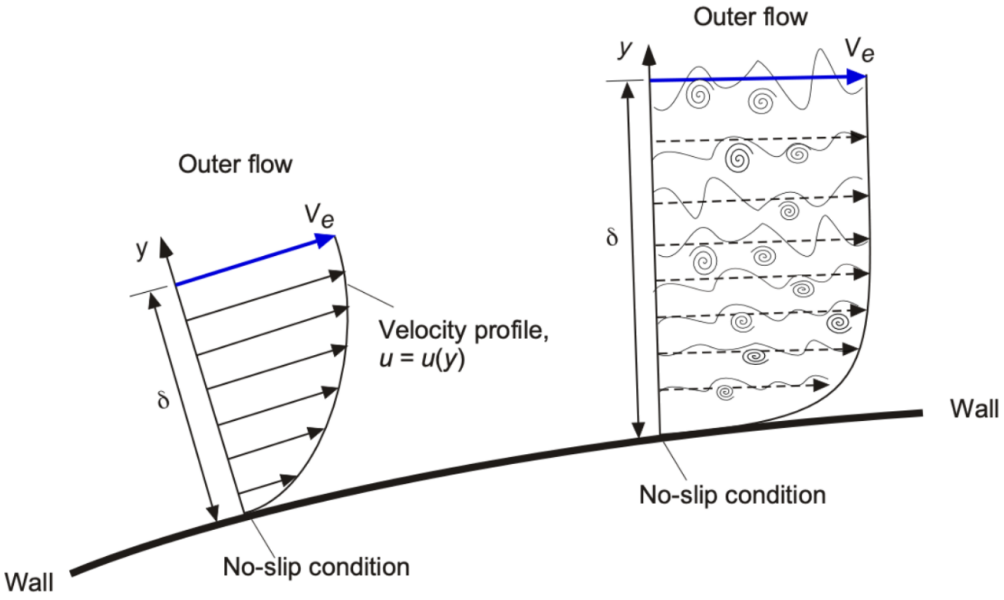

Figure 3: The different flow patterns compared between laminar and turbulent flow on a wall with no-slip condition. On the left laminar flow is represented and on the right, turbulent flow with the higher formation of eddies, taken from [23].

In order to approach trailing edge noise, the airfoil shape itself has been considered. The airfoils of functioning wind turbines are often custom, beginning from a standard NACA foil shape [24]. This foil shape is the plane of the tip design, an example is provided in Figure 2 [19]. The trailing edge flow is the final surface whereby the air interacts with the blade. As shown in the figure, the laminar flow along the blade transitions to turbulent flow at a certain point after the leading edge [19; 23]. This point tends to be determined primarily by the Angle of Attack (AoA). This angle is the angle at which the wind hits the airfoil and is responsible for determining how thick this boundary layer becomes. The thicker the boundary layer, the more turbulent the flow becomes as demonstrated in Figure 3. Therefore, addressing the thickness of the boundary layer is directly related to the noise produced [19].

Furthermore, the thickness of the boundary layer can also be related to the smoothness of the surface. The smoothness, or rugosity of the surface, is relevant for developing a better flow pattern for the air. If, for example, there was a raised piece on the wall shown in Figure 3, the flow pattern would be further disrupted on the wall, causing more disturbances behind the blemish [25].

2.2 System Description

As discussed, frequently power reduction is the current solution to the noise problems of wind turbines [9]. However, given the increasing demand for a solution, more research has been dedicated towards finding a suitable trade-off between efficiency and noise. On the mechanical side, new damping solutions have been introduced, which are able to suppress the noise

produced by the drivetrain [19; 26]. These types of solution often stem from their own sectors improving rather than focusing specifically on reducing the noise of wind turbines [26]. However, on the aerodynamic side, the goal is specific to the turbines themselves given that this flow pattern is unique to wind turbines. With this, the biggest potential lies in the angles and shape of the blade, as these are the most related to the flow pattern, which is responsible for the production of noise [19; 24].

The basics of wind turbine design focus on the shape of the airfoil along the blade, but also can look at the uniformity of the blade [19]. For example, with the rise of bio-based design, inspiration from owls and mosquito species has led to serrations being an interesting solution to noise [27]. Other studies focus more on the airfoil shape itself, investigating whether a change in the entire trailing edge design can be better optimized for noise without a significant trade-off with efficiency [28]. However, a key area lacking is the combination of different influential factors in simulations. Combining factors such as shapes and angles, as well as other factors such as the wind direction and blade rugosity, other major contributors to the noise situation of a wind turbine, is something which can be better explored.

With the current state-of-the-art and research pathways in mind, a system diagram was constructed in Figure 4, which first analyzes the relevant internal factors pertaining to the wind turbine noise production. This system was constructed with four instruments based on where the biggest potential lies to improve the three metrics on the right-hand side of the diagram.

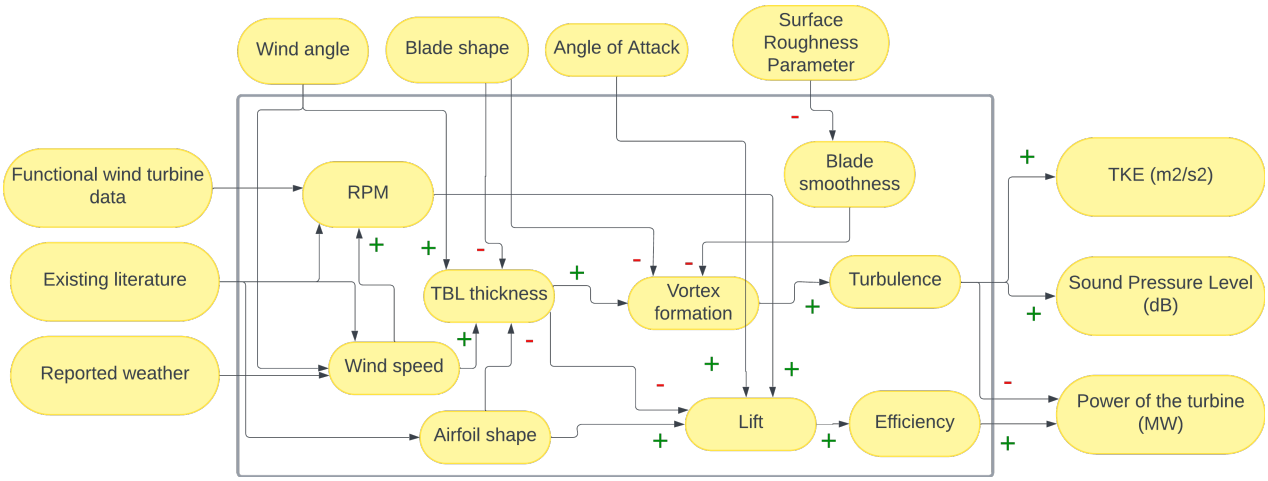

Figure 4: System description of the project. The interacting elements are shown within the box, with the external factors placed on the right of the box, the instruments above the box and the metrics on the left of the box.

In Figure 4 the tested parameters are listed as the wind angle, blade shape, AoA and the surface roughness parameter. Within the system itself, a number of the elements are clearly linked to a higher degree. The most important of which is the turbulence that is directly related to the main metrics of TKE and SPL [21]. However, turbulence has only one internal link in the system, which is vortex formation. More vortex formation produces more turbulence. The dynamics of the vortex formation connects many more of the system elements. Especially those that arise from the instruments.

One of these is the shape of the blade, which is the key focus of the research, as it has

the greatest potential impact on the formation of vortices [28]. The wind angle has an influence on the inlet parameters and is only linked to these elements of the system. It relates to the RPM of the turbine and the inlet velocity. These two parameters could be changed but instead are selected to remain constant for this study. The wind velocity and RPM effects the amount of lift produced, affecting the efficiency in general. This creates a higher power output turbine. The AoA also plays a larger role in efficiency, with some airfoil shapes helping to produce more lift up to around 25 degrees. However, the more it rotates, the more drag is produced. This means that a suitable angle generally falls between 5 and 20 degrees for the AoA [29]. The AoA will be investigated with literature hand in hand with the blade shape due to the dependency and direct relation between these two variables.

The final important instrument in this research is the surface roughness parameter, or the rugosity of the blade. The general relation between the noise and efficiency of a blade and its roughness is that with higher roughness there is a higher amount of vortex formation [25]. However, the extent to which this can be manipulated and the extent to which the relationship affects the noise is not yet fully developed. This makes it an important parameter to add to the study to investigate more realistic patterns of noise formation and look at how this parameter is influenced by the other tested parameters.

2.3 Research Objective

This project aims to develop a wind turbine simulation design that addresses the aerodynamic noise problem while maintaining turbine performance. This design will arise from investigating different parameters as discussed in the system description. This will be done to further explore the way these factors influence each other in decreasing noise. Given that the greatest sound problems prevail at the tip of the blade [19], the research will focus on understanding the flow patterns at the blade tip, and how these can be improved, especially in terms of noise. This additionally requires then a focus on being able to translate pressure and velocity field values produced by simulation into noise values measured in dBA. This will be solved through the use of the intermediary step of the turbulence kinetic energy (TKE). Using computational fluid dynamics (CFD) as a simulation tool as well as computer-aided design (CAD), a design will be developed in order to improve the noise produced by the turbine. The TKE will be measured in COMSOL Multiphysics ®, whereas the SPL will be approximated with MATLAB. The suggested designs will also be tested through the use of a flow tank. In order to make the goal measurable, an improvement of 3 dBA will be the goal, as this is a measurable quantity that also fits within the range of possibility in accordance with Figure 1. The purpose of the research can be summarized in the following objective statement:

Goal Statement

To develop a complete wind turbine SST simulation which measures the effects of blade shape, angle of attack, wind direction and surface roughness on the TKE produced by the wind turbine. This data will then be used to test which designs provide 3 dBA noise reduction in terms of Sound Pressure Level.

2.4 Research Questions

This goal will be obtained by answering a series of research questions that reflect the desired outcome of the project.

What blade design varied by the parameters angle of attack, wind angle and blade rugosity offers a 3 dBA improvement to the Sound Pressure Level produced by a wind turbine?

SQ1: Which airfoil shape from the NACA database is most suitable to base the design of an improved blade on?
SQ2: What role does rugosity play in the formulation of turbulence and how can this variable be tested to offer some parallels to reality?
SQ3: What contribution does the wind angle have on the noise produced by a wind turbine and how can it be combined with the other parameters to analyze the noise production?
SQ4: How can the blade design best utilize the angle of attack to increase the lift while minimizing noise?
SQ5: How can a flow tank be configured and used to aid the results found computationally and to draw conclusions about the shape of the blade?

These questions incorporate each of the instruments defined in the system in order to find their relationship to the metrics.

3 Design

3.1 Numerical Method

In order to be able to apply each of these mathematical models in simulation, Computational Fluid Dynamics (CFD) will be used. CFD is governed by the Navier-Stokes equation, as detailed above [21]. There are varying approaches to CFD, starting with the way in which the model generates the turbulence. In the case of wind turbines, there are two main methods applicable, the Large Eddy Simulation (LES) and Reynolds-Averaging Navier Stokes (RANS) approach. LES directly resolves the larger turbulent structures while modeling the smaller ones to capture more detailed transient flow behavior. On the other hand, RANS averages the effects of turbulence over time to solve for mean flow characteristics. LES is higher in turbulence resolution in exchange for being more computationally demanding; however, RANS is efficient in predicting the overall performance and long-term behavior of the turbine [30].

This study will utilize RANS as the approach to CFD simulations, as it has several different models, which can help to provide higher turbulence resolution at lower computational cost. The two most utilized RANS models are the kappa-epsilon (k-ϵ) and kappa-omega (k-ω) models. The kappa (k) is the TKE whereas the other variable is the dissipation rate. The two models vary in dissipation rate; the k-ϵ model is utilized for larger flow models with high Reynold's numbers; it is mostly suitable for general flow but less accurate near walls. On the other hand, k-ω is much better at accurately predicting turbulence near walls and at the boundary layers. There are also more RANS models, in particular the SST model which combines the best efforts of the k-ϵ and k-ω models [30]. With this combination of strengths, the SST model offers the best definition of turbulence and will be used for the simulations.

The SST model is defined in the following two equations, the first describing the TKE term 'k', and the second describing the specific dissipation rate 'ω' [30].

$$\frac{\partial(\rho k)}{\partial t} + \frac{\partial(\rho u_j k)}{\partial x_j} = P - \beta^* \rho \omega k + \frac{\partial}{\partial x_j}\left[(\mu + \sigma_k \mu_t)\frac{\partial k}{\partial x_j}\right] \tag{5}$$

$$\frac{\partial(\rho \omega)}{\partial t} + \frac{\partial(\rho u_j \omega)}{\partial x_j} = \frac{\gamma}{\nu_t} P - \beta \rho \omega^2 + \frac{\partial}{\partial x_j}\left[(\mu + \sigma_\omega \mu_t)\frac{\partial \omega}{\partial x_j}\right] + 2(1 - F_1)\frac{\rho \sigma_{\omega 2}}{\omega}\frac{\partial k}{\partial x_j}\frac{\partial \omega}{\partial x_j} \tag{6}$$

The relevant variables to define are the production term 'P', the Reynold's stress tensor 'τ_{ij}' and the Strain rate tensor 'S_{ij}' [30].

$$P = \tau_{ij}\frac{\partial u_i}{\partial x_j} \tag{7}$$

$$\tau_{ij} = \mu_t\left(2S_{ij} - \frac{2}{3}\frac{\partial u_k}{\partial x_k}\delta_{ij}\right) - \frac{2}{3}\rho k \delta_{ij} \tag{8}$$

$$S_{ij} = \frac{1}{2}\left(\frac{\partial u_i}{\partial x_j} + \frac{\partial u_j}{\partial x_i}\right) \tag{9}$$

The Reynold Stress Tensor, τ_{ij}, can also be further simplified to not include compressibility effects given the assumption of incompressible flow. Then the term $\frac{2}{3}\frac{\partial u_k}{\partial x_k}\delta_{ij}$ becomes zero as

$\nabla \cdot u = 0.$

These equations will be utilized within the computational domain. The software which will be used for CFD is COMSOL, which has the SST model as part of the RANS turbulence model. COMSOL utilizes Finite Element Method (FEM) in solving the simulation. FEM is used over Finite Volume Method (FVM) for this study due to the coupling of the results to acoustic modeling, as discussed in the following section. Furthermore, the use of complex geometries in some of the design phases also allows greater precision in solving when working with elements rather than through control volumes as FVM does [31; 32]. These simulations will be run under frozen-rotor conditions, in order to be able to accurately depict the turbulence surrounding the blades but with eased computational conditions [33].

3.2 Modeling Noise

In order to be able to find the SPL, the N-S equation needs to be transformed into data that can be interpreted using decibels. This can be done with the long-standing method of the *Ffowcs Williams-Hawkings Equation* (FW-H) [34]. Using the N-S equations (equations 1, 2 3), Ffowcs, Williams and Hawkings developed the following equation for measuring the Sound Pressure Level (SPL).

$$\begin{aligned}\frac{1}{c_0^2}\frac{\partial^2 p'}{\partial t^2} - \nabla^2 p' = &\frac{\partial}{\partial t}\left[\left[\rho_0 v_n + \rho(u_n - v_n)\right]\delta(f)\right] \\ &- \frac{\partial}{\partial x_i}\left[\left[p_{i,j} n_j + \rho u_i (u_n - v_n)\right]\delta(f)\right] + \frac{\partial^2}{\partial x_i \partial x_j}\left[T_{ij} H(f)\right]\end{aligned} \tag{10}$$

The left-hand side of the equation is described as the wave operator. This describes how the sound waves propagate through the medium, primarily the fluid. On the right-hand side of the equation there are the three contributions to sound. The first term, which is controlled by a time derivative, is the monopole term. This measures the sound of any monopole effects from volume changes in the fluid. The following term is the dipole term, which looks at the interaction of the fluid on the surface of the blade and the noise that this produces [34]. The final term, with the stress tensor T_{ij}, is the quadrupole term, which measures the noise effects of turbulence in the fluid itself, making it one of the most important terms of the equation. The stress tensor T_{ij} is central in the relation of noise to turbulence in the FW-H analogy [34; 35]. It accounts for multiple contributions from fluid motion, Reynolds stresses, pressure fluctuations, and viscous stresses, shown in the following expansion:

$$T_{ij} = \rho u_i u_j + \left(p' - c_0^2(\rho - \rho_0)\right)\delta_{ij} - \sigma_{ij} \tag{11}$$

Where, the viscous stress tensor, σ_{ij}, is expanded as:

$$\sigma_{ij} = \mu\left(\frac{\partial u_i}{\partial x_j} + \frac{\partial u_j}{\partial x_i} - \frac{2}{3}\delta_{ij}\nabla \cdot \mathbf{u}\right) + \lambda\delta_{ij}\nabla \cdot \mathbf{u} \tag{12}$$

This tensor can be simplified under the incompressibility assumption, yielding [35; 34]:

$$\sigma_{ij} = \mu\left(\frac{\partial u_i}{\partial x_j} + \frac{\partial u_j}{\partial x_i}\right) \tag{13}$$

Each contributor of the FW-H equation affects the total SPL differently. For example, monopole noise is dominant in cases of large-scale volumetric changes, such as blade passage effects. Dipole noise arises from blade-fluid interactions, such as aerodynamic forces and shear layers. Quadrupole noise is significant in highly turbulent flows, especially at high wind speeds or around blade tips, given the presence of the stress tensor [35].

Other variables are defined as follows.

- p': Acoustic pressure fluctuation
- c_0: Speed of sound in air at 100m altitude and 15 °C ($343 m/s$)
- ρ_0: Density of air at 100m altitude and 15 °C ($1.22 kg/m^3$)
- u_n, v_n: Normal velocity components of the fluid and boundary surface.
- f: Level set function defining the surface geometry.
- $\delta(f), H(f)$: Dirac delta and Heaviside functions that define the boundary and volume.

The integration of noise predictions begins with the outputs from the SST turbulence model, which resolves the pressure and velocity gradients ($p, \nabla u, \nabla v, \nabla w$). These resolved flow fields are used in the SPL equation to calculate acoustic predictions, transforming them into SPL estimates. The rotating domain of the turbine introduces additional factors, such as Doppler effects and tip noise, which are captured by the dipole and quadrupole terms [36]. The transient nature of noise is accounted for with the time derivative. However, given the use of a frozen rotor simulation, these will be omitted from the final SPL analysis. Furthermore, the calculated SPLs are scaled to standard metrics by calculating with A-weighted SPL, producing values in dBA. These metrics help to provide data relative to human hearing standards [36].

Deriving the SPL from the FW-H equation is calculated as [36]:

$$SPL = 20 \log_{10} \left(\frac{|p'|}{p_{\text{ref}}} \right) \tag{14}$$

Where the reference pressure is $20 \cdot 10^{-6}$ Pa [36].

3.3 Boundary Conditions

The following stage of the modeling is to select the best boundary conditions given the varying parameters that will be tested within them. The inlet velocity of the wind will be a set parameter and is set to 12 m/s, based on the measured averages as well as other studies which use a wind speed between 7 and 15 m/s [37]. Furthermore, it can be observed that 12 m/s is considered the nominal wind speed, as demonstrated in Figure 1 [8], after which the effect of the wind speed is negligible on the power output [38]. The simulation will presume incompressible flow since the velocity of the wind will not exceed this 12 m/s, meaning that the Mach number will not exceed 0.05, permitting the same assumption made earlier in Chapter 2.

The outlet is on the opposite side of the turbine and is a pressure controlled boundary. The other surrounding surfaces are open boundaries or symmetry, with the exception of the side below the turbine itself, which supports the stem. This boundary is a wall, along with the stem and the turbine itself, as shown in Figure 5 [38]. The same set up will also be

used to test the rugosity as a parameter, despite the fact that in Chapter 2 the stem is not as interesting because it does not contribute to the noise as much compared to the blades [25]. However, testing which effects it has remains important for gaining insight into the full picture. The stem will also accumulate particles over time, which means it should also be included in the simulations.

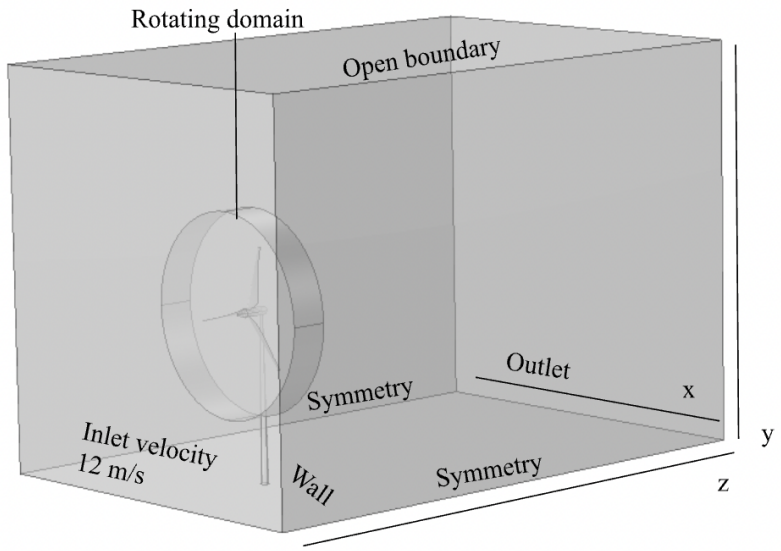

Figure 5: The boundary conditions of the simulation set up represented visually.

Furthermore, Figure 5 also refers to a rotating domain around the turbine itself. A defined cylinder will be the specific 'rotating domain' in which the moving mesh is located. This accounts for the movement of the turbine, without rotating the stem as well. This rotation will be constant, with the rotations per minute (RPM) of the turbine set to 11 RPM because this is the RPM achieved with the defined inlet velocity. This also reflects the RPM of the turbine with the nominal wind speed, a constant rotational speed. Above this nominal wind speed, the RPM does not increase, meaning that this value is effectively representative of the fastest speed at which on shore turbines operate [8].

3.4 Airfoil Shape

The base case of the design will be a NACA 2412 foil. The parameters defined in the system do not focus on altering or redesigning the airfoil shape; therefore, this shape will remain constant unless slightly altered while looking at the entirety of the blade design. The NACA 2412 foil is often used as the starting point in papers and for real turbines given its appropriate ratio of lift to drag. In addition, its selection was based on a comparison of some of the airfoil example shapes that often appear in articles [39; 40]. The airfoil shapes most frequently used in research are the NACA 4405, 0012 and 2412 shapes [40]. Using XFLR5, a program that can compare the 2D airfoil shape for a number of parameters related to lift, drag, and AoA, these three shapes were tested for their range. Given that AoA is the main parameter that relates to the shape of the airfoil, it is the most important to test for performance. In Figure 6, the change in efficiency measured by the lift/drag coefficient is plotted against the AoA.

The AoA of the 2412 foil shape can suitably range up to 15 degrees without sacrificing a significant amount of the performance. Although its peak efficiency is lower than that of the

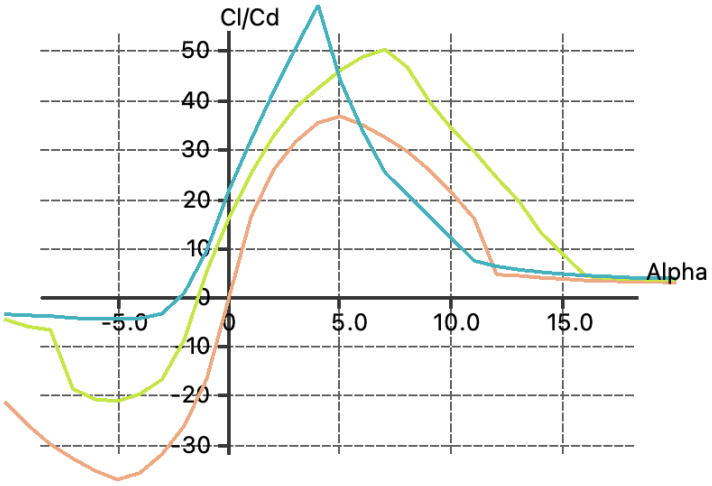

Figure 6: Comparison of the 4405 (blue), 0012 (red) and 2412 (green) airfoil shapes by plotting efficiency against AoA.

4405 profile, it has less dramatic performance for other angles of attack. The 4405 profile is an airfoil optimized for performance at one AoA. With the goal of testing multiple AoAs, this profile is not suitable. The 0012 profile has a more balanced performance, enabling it to operate with a negative or positive AoA. Although similar performance in both directions can be useful, the efficiency is not very high as shown in Figure 6. This efficiency is similar at each of the opposite peaks, making the expected difference from testing two different AoAs little to none. With the more evenly spread profile of the 2412 profile and relatively high peak performance across varied angles, it is the preferred selection of airfoil shape in this research.

3.5 Parameters

3.5.1 Angle of Attack

The AoA is one of the parameters that has the largest trade-off between sound and efficiency. Increasing the AoA leads to an increase in lift acting on the blade; however, the drag also increases. This relation is not necessarily proportional, with a larger range in which acceptable values can be found, highly dependent on the shape. As discussed in the previous section, the selected airfoil choice is a NACA 2412 profile. The data collected for Figure 6 in XFLR5 shows peak performance of the 2412 profile at a 7 degree rotation. This will be the first AoA to be tested, but, to look at how important the AoA is, another value should also be tested. For this other value, a higher AoA will be chosen, as the range of values often lies between -10 and 20 degrees (depending on the airfoil shape). However, the efficiency of the profile drops off quickly while approaching 20 or -10 degrees. The most suitable value that also tests a larger difference is at 12 degrees. This makes the two selected AoA to test **7 and 12 degrees**.

3.5.2 Blade Shape

Larger amounts of research have begun investigating designs to reduce turbine noise by just one or two dBA to meet noise quotas [28]. In this research, attention falls on how the formation of vortices can be best disrupted to cause less noise. The disruption of the constant patterns can best be achieved by alterations to the geometry. These alterations eventually result in constant patterns as well, but with a lower TKE value to accompany them, meaning a

reduction in noise. However, at the same time the efficiency of the aerodynamic performance must not be compromised. These can best be avoided by alterations in the direction of the airfoils (x-axis direction) rather than perpendicular to the airfoil shape [28]. Some research has focused on this approach on the perpendicular axis, looking at winglets as a potential solution [41]. Winglets are used in aircraft design, placed on the tip of the wing which extends upward, outward, or sometimes slightly inward. It often appears as a sharp fin structure. It is designed for efficiency purposes rather than to reduce noise, but typically these go hand in hand given their relation to turbulence. The winglet works to enhance efficiency by minimizing the drag generated by vortices at the edge of the blade, similar to the problems that wind turbine blades face [41].

Winglets go in a perpendicular direction to the airfoil shape. But, as mentioned, parallel additions are more friendly for supporting a solution that is aerodynamically optimal and reduces noise. These types of alterations in the geometry can be taken in several different directions. The first thing to consider is adding to the geometry versus taking away from it. Additions can be costly but do not alter current structures and risk damaging structural integrity. In this way, removals are a bigger challenge as taking away from already built structures is virtually impossible without needing to fully inspect before rehauling the design.

Looking at additions similar to the winglet but rather in the direction of the airfoil profile leads to a fin design. A fin placed along the edge would be expected to yield a similar disruption in vortices, but to a lesser extent than the winglets. The winglets are superior in disrupting the vortices given the dramatic change taking place; however, this would be expected to be counter productive for the sake of noise. A fin at the tip of the blade that is able to replicate the effects of a winglet would be ideal, and hence a useful blade shape to test.

With looking into designs which are able to disrupt the vortices, lots of research turns towards busy geometries along the trailing edge of a blade. Brushes and serrations have had upswing in their effectiveness in reducing noise [19; 42; 28]. These disruptive geometry styles are capable of disrupting and scattering turbulent airflow patterns. The sharp contrast where the smooth blade surface meets the passing air along the trailing edge is highlighted as the primary noise maker. When used in a uniform and well positioned manner, the intensity of the interaction between the blade and air can be broken by making it a more gradual transition. This reduces the intensity and coherence of noise-producing vortices. Furthermore, serrations can act as multiple smaller edges, which may be able to diffuse sound waves and lower the overall noise intensity [19].

2D Design for Selecting Blade Shapes

To investigate which blade shapes have the most potential to reduce noise, several different designs can first be tested in a 2D domain before moving to the 3D domain. Therefore, a complete 2D design based on a slice of the 3D model was constructed. A 2D design is much less computationally demanding, especially when it comes to time-dependent parameters. 2D designs were initially run with the profile collected from a 3D model, which takes into account the angle of the blade on the z-axis. However, in order to be able to measure the improvements expected from the blade shape, a zero-degree AoA is needed. The zero-degree AoA uses the largest area of side profile.

Figure 7 shows the largest area slice with a zero degree AoA. The figure shows the results of running the simulation time dependently with the results showing after 30 seconds. The plot

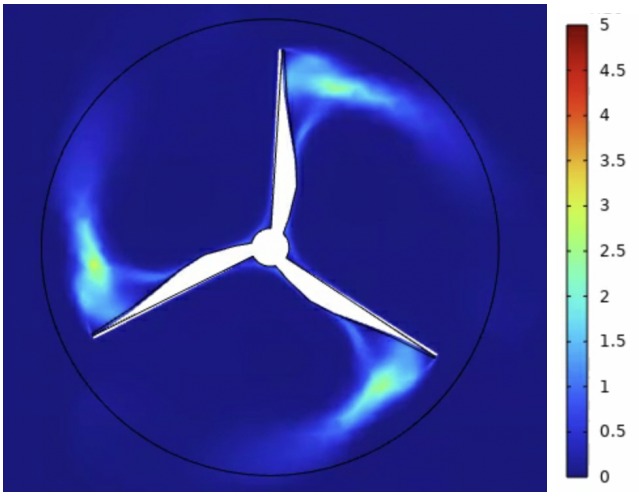

Figure 7: Base case slice of the 2D model

shows the results in terms of TKE, with a scale ranging from 0(blue) to 5(red) x 10^{-2} $\frac{m^2}{s^2}$, given the smaller scale nature of the 2D model.

With a standard case to compare to, different geometrical additions were tested to determine their abilities to reduce the TKE. A selection of these different simulation results are shown in Figure 8.

Of the six cases presented in Figure 8, most relate to the addition of serrations or geometric placements on the tip of the blade. The top three simulation sets show varieties in serration types, with varying serration length and varying lengths of placement along the turbine. The short serrations shown in Figure c produce a more intense turbulence spot than the base case in Figure 7, as well as more intense turbulence from the trailing edge along the blade. The extended length of serrations similarly results in more turbulence along the entirety of the trailing edge in a sweep like motion. In Figure b, it is clear that three sweeps of vortex formation are taking place along the blade. Figure a shows higher serrations, but not over an extended blade length. While there is formation of turbulence along the entirety of the trailing edge, this is at much lower intensity to the two other serration configurations as well as the base case slice.

The three bottom results show the effects of adding different geometries to the tip of the blade. The first of which is the addition of a right-angled fin, after configuring with different ratios of the fin, the best performing fin of a right-angled shape used a ratio of 1.625 to 1 in height to length. This geometry was able to produce the least turbulence in all of the simulations tested in 2D. Although moving to the 3D domain may alter the way in which the fin is effective, compared to the other geometries tested with a similar set up, it yielded hopeful results. The other figures, which utilized a block with a rounded edge and a larger block with a rounded edge, did not have the same effectiveness as the fin. These results indicate that the straight line on the tip of the wing produced better aerodynamic results and less turbulence, rather than a rounded structure.

With the 2D results, the best found blade shapes to test in simulations are a shape with less rotation in the blade, but no additions in geometry. Secondly, serrations on the final quarter of the blade with a length to width ratio of 1.5 and finally, a fin shape with 1.625 to 1 ratio. These will be the three main cases explored in the Results chapter.

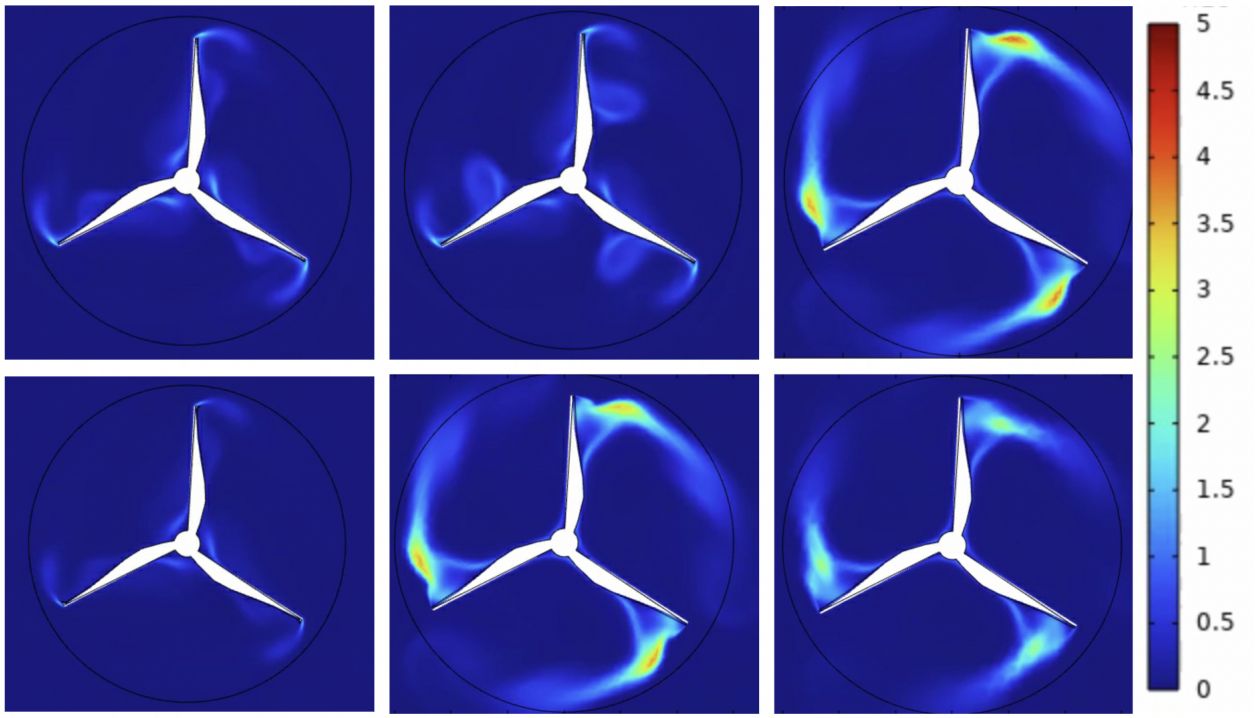

Figure 8: Six different blade geometry tests, from top to bottom, left to right: a. Serrations placed on a reduced blade length with a 1.5:1 height to length ratio. b. Serrations placed on an extended blade length with a 1.5:1 height to length ratio. c. Serrations placed on a reduced blade length with a 1:1 height to length ratio. d. Right angled triangle fin placed at the edge of the tip with a 1.625:1 height to length ratio. e. Rectangular block with circular edge placed at the edge of the tip with a 12.7:1 height to length ratio. f. Rounded edge placed on the tip.

3.5.3 Wind Angle

In order to change the angle of the wind, this can be altered through making a union between a cylinder and the block surrounding the wind turbine, as shown in Figure 9. Then, the inlet can be changed along the cylinder's surface. The angle can be adjusted by first defining the velocity as U_{inf} in the parameters. Based on simple 3D geometry tests, a 45 degree angle rotation from the blade and wind directly perpendicular to the blades produced the more interesting results in terms of TKE over the entire volume. This will be reproduced by applying the wind from the right-hand side, assuming that the results would be identical if the rotating domain was made clockwise for left-hand wind.

3.5.4 Blade Rugosity

The blade rugosity choices for the parameters stemmed primarily from studies in literature that focused on the effects of tripping the blade. This can be implemented into the study by changing the conditions of the walls in the study to have roughness. For the complete set of simulations that will be tested, the two most important conditions are relevant and will be tested when it comes to blade rugosity. The first of which is the non-tripped blade, which will have no-slip as a condition on each of the 'wall' surfaces. This includes the stem of the blade, but most importantly the blades themselves and the generator structure center of the blades. This condition is tested because it best represents the ideal scenario of turbine operation and will predictably have less turbulence and, therefore, noise given the lack of extra divots (see Figure 3).

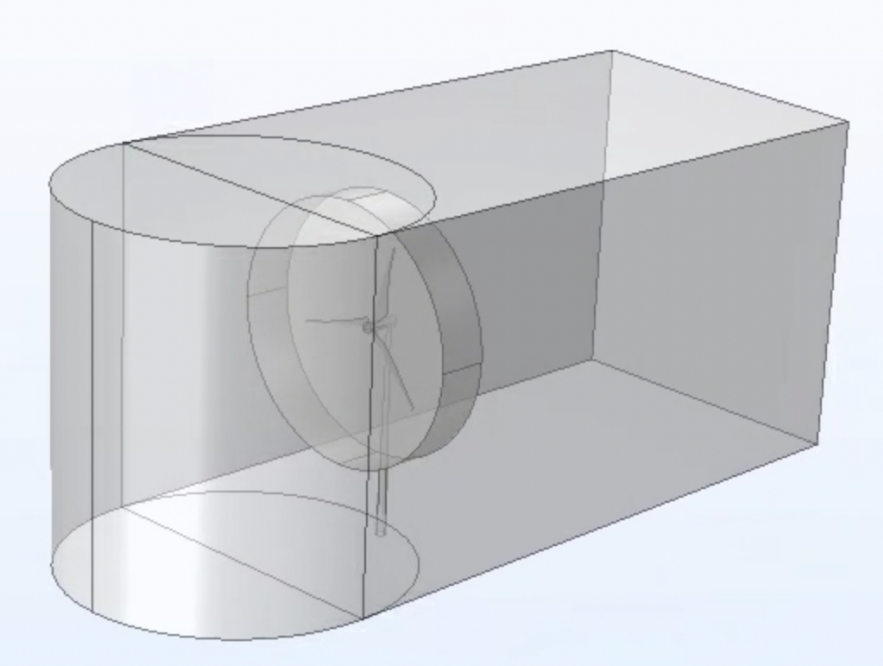

Figure 9: The adjusted boundary conditions to account for changing the wind angle.

In order to also represent the more realistic scenario over time, a tripped version of the blades will also be simulated. Over time, turbines are more likely to accumulate particles and a rougher surface due to their constant operation. This will be computationally tested using the $k-\epsilon$ turbulence model as opposed to SST, since it allows for equal surface roughness to be modeled on all defined walls. This is a more accurate representation of the realistic effect of roughness on wind turbines to be modeled. Sand roughness can reflect this in the model, which will be set to a lower roughness level of 10 μm [43].

The $k-\epsilon$ model is similar to the SST model in regard to the equation for k. The only exception is the $\beta^* \rho \omega k$ term, given that the ω term is obsolete in the $k-\epsilon$ model. This is the transportation term in the model and is replaced with the ϵ variable, which has the limitation that it is less accurate next to walls, as described in the sections above. The equations for the $k-\epsilon$ model are shown below.

$$\frac{\partial(\rho k)}{\partial t} + \frac{\partial(\rho u_j k)}{\partial x_j} = P - \epsilon + \frac{\partial}{\partial x_j}\left[(\mu + \sigma_k \mu_t)\frac{\partial k}{\partial x_j}\right] \tag{15}$$

$$\frac{\partial(\rho \epsilon)}{\partial t} + \frac{\partial(\rho \epsilon u_i)}{\partial x_i} = \frac{\partial}{\partial x_j}\left[\frac{\mu_t}{\sigma_\epsilon}\frac{\partial \epsilon}{\partial x_j}\right] + C_{1\epsilon}\frac{\epsilon}{k}2\mu_t E_{ij}E_{ij} - C_{2\epsilon}\rho\frac{\epsilon^2}{k} \tag{16}$$

Where, E_{ij} represents the component of the rate of deformation, and μ_t represents the eddy viscosity, reflected in $\mu_t = \rho C_\mu \frac{k^2}{\epsilon}$.

3.6 Simulations

The next stage is to combine these parameters into a set of simulations which appropriately reflect the goals of the research. The purpose of the system is to investigate the parameters, but this also requires a combination of the parameters and how they influence each other.

Table 1: Overview of the simulations which will be used to explore and test the parameters of the study.

Simulations	Basic optimised shape	Blade with fin	Blade with serrations
1-3	7, nt, front wind	7, nt, front wind	7, nt, front wind
4-6	14, nt, front wind	14, nt, front wind	14, nt, front wind
7-9	7, t, front wind	7, t, front wind	7, t, front wind
10-12	7, nt, right wind	7, nt, right wind	7, nt, right wind

4 Computational Results

This chapter presents the outcomes of the design simulations conducted. The previous section used 2D simulations to set up the selection of blade configurations. These will be expanded into 3D geometry beginning with an initial base case blade.

The simulation setups, as summarized in Table 1, systematically explore different configurations, including the basic optimized blade shape, blades with fins, and blades with serrations. For each configuration, varying wind directions, rugosity, and wind speeds were tested.

4.1 Base Case

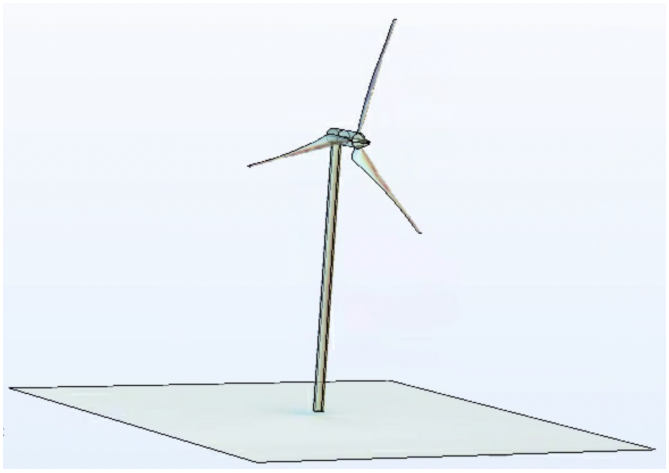

Figure 10: The entirety of the wind turbine walls boundary, adapted from an online CAD model

In order to improve the design, the initial design will first be run to be able to compare the results. The base case is the simulation run with front wind, a smooth blade, 7 degrees AoA and the same airfoil profile. This blade design was taken from a previously made CAD blade. This blade has a higher degree of rotation along the blade as compared to the new proposed designs. The additional geometry such as the stem and the box for the mechanical elements is also derived from the same CAD model previously made. The full model is shown in Figure 10 where the model is shown only with the walls, without the accompanying boundary layers for the air like in Figure 9.

Figure 11: TKE plotted along one of the three blades. More intense turbulence is located on the trailing edge and the tip of the blade in the light blue shade and higher concentrated contour lines.

The first important parameter defined is the TKE which is shown in Figure 11 along the blade. The leading edge is found to have some of the more prevalent spots of turbulence,

which are about equally distributed along the blade. There is a higher concentration of turbulence at the tip of the blade, as is expected with what is understood about vortices and what is found in literature. In Figure 12, some of the flow patterns which are responsible for this turbulence are shown with streamlines. The streamlines are focused on the two edges of the blade, including the side which is attached to the center structure. Figure 11 also shows a minor increase in TKE at the leading edge as well as some higher turbulence peaks at the thickest point on this edge. However, this flow pattern is not necessarily responsible for a large production of TKE, it simply indicates a more intricate flow given the geometry present. On the other hand, at the tip which is not supported or attached to any structure is where the increased concentration of streamlines is more interesting. Figure 12b shows the flow wrap around the airfoil shape before continuing. This flow pattern shows how a dramatic difference in pressure between the two sides of the blade was created, which results in higher vortex shedding, and hence, more turbulence at this area.

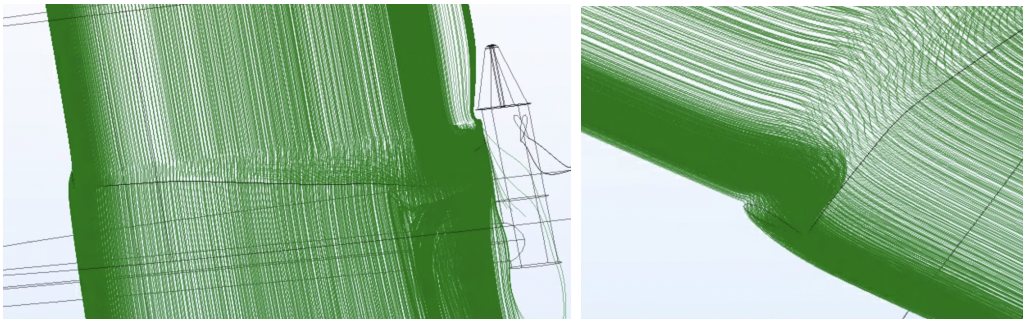

Figure 12: Concentration of flow at both sides of the blade on the end as well as a greater focus on the flow patters at the blade tip in image b.

This higher concentration of turbulence at the tip of the wing causes larger vortex shedding behind the blade as well. This is shown by looking at the velocity profile, which when highlighting the streamlines shows the formulation of eddies at the tip of the blades. The streamlines flow over the blade itself, which is shown with their vertical nature in the center of Figure 13. The left-hand side of the image shows some curve in the streamlines given the center box being near. Also demonstrated with the larger patch of blue present underneath showing a dramatic fall off in velocity nearer to the center. This is expected given the centrifugal forces and the fact that the slice of data is taken closer to where the beginning of the blade is present.

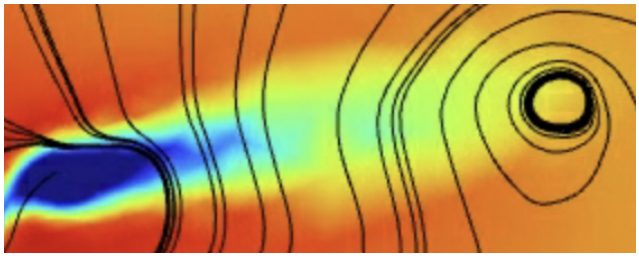

Figure 13: Velocity plotted half a meter behind a single turbine blade showing the formation of vortices behind the single blade.

This model was initially validated by comparing the efficiency values with the literature. This is done by integrating the pressure coefficient value on the surface of the turbine. This produces values that are mainly within the range of -0.05 and 0.05, which is consistent with the

experimental results found in a similar computational study carried out by Hohlfeld [44; 45]. With similar values obtained, the model is sufficient in providing a base on which to build on.

4.2 COMSOL Data

The first set of simulations stem from adapting the twist and scaling the uniform 2412 airfoil shape along the blade. However, this shape is still referred to as the basic shape between the three improved shapes. This is because, in addition to improving the profile along the blade, there are no geometric changes or additions. This shape is constructed using SolidWorks, with a lower amount of rotation along the blade than the base case, as well as a larger surface area at the tip of the blade, which can attribute to the lift ratio. But, more importantly should reduce the noise produced by the blade. This improvement can be linked to the extension of the laminar boundary layer with less rotation along the blade. Immediately in the flow data shown in Figure 14b, it is clear that the edge of the surface is more standardized in terms of flow shapes. There is no longer more dense flow patterns at the tip of the blade. This does not necessarily mean less turbulence in the flow, but simply that the velocity along the edge of the blade is less complex.

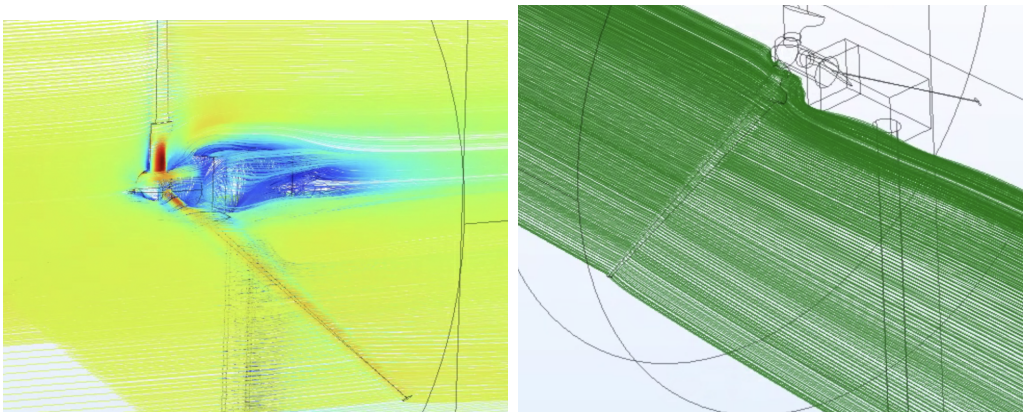

Figure 14: Streamlines plotted on the improved basic shape case. Figure a. The velocity over a blade and the gearbox of the turbine. Figure b. The concentration of streamlines along a blade, not corresponding to their value.

The basic shape has the upper hand in this manner over the two other tested shapes. The fin and serrations both show that a fairly complex flow pattern reaches the tip, where the additional geometry comes into place. However, this is expected to be able to decrease the TKE and noise patterns by disrupting the formation of continuous problematic eddies and wakes from the blade. In Figure 15, a comparison between the three shapes is shown side by side, all with an AoA of 7 and smooth blades; the TKE patters along one blade are shown in detail. Each of these have different scales due to the capabilities of COMSOL but can still be analyzed for their varying values along the blades. The basic shape blade has the least TKE, which likewise to the two other blade shapes has a higher peak two thirds down the blade. It is not immediately clear why a higher source of turbulence occurs at this point in the leading edge. Its similarity across all three indicates it could have to do with the decreased amount of rotation in the blade.

The fin blade configuration shows a sharp concentration of turbulence along the surface of the inside of the fin. This reaches 3.52 m^s/s^2, which is much higher than the peak values

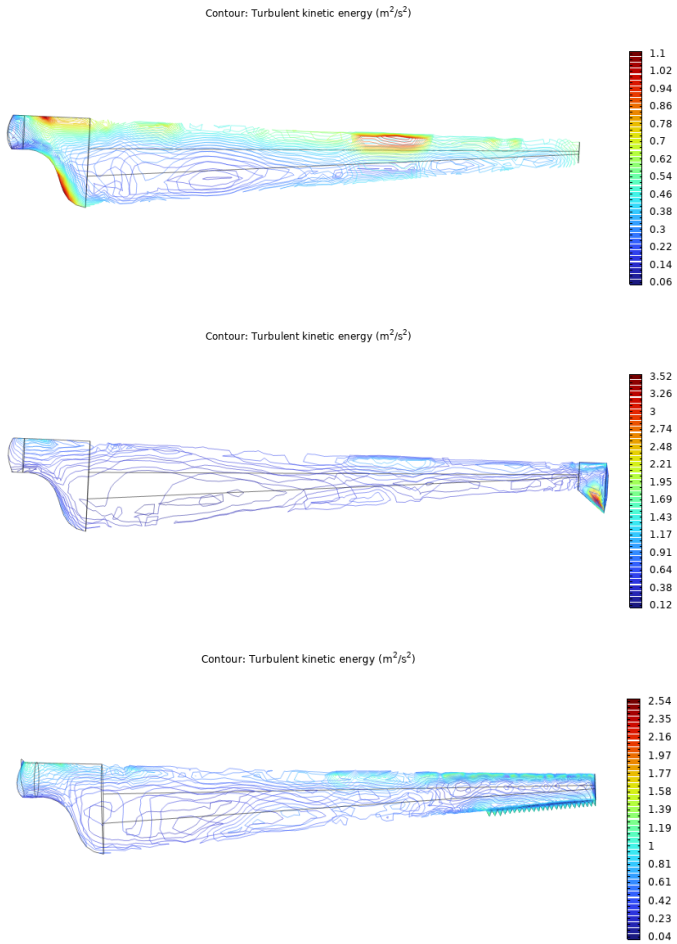

Figure 15: Comparison of the three blade shapes in terms of TKE along the surface of one blade. This is represented by contour on the blades themselves.

on the basic blade shape. The rest of the blade is similar to the basic shape, with most values floating around 1 m^2/s^2. This is expected since the geometry is only changed at the tip between these two designs. However, it will then be up to the extracted SPL data to reveal whether the higher TKE on the surface of the blade is worth anything for decreasing the sound in the wakes behind the blade.

The serration shape lies somewhere in between the fin and the basic shape in terms of the maximum TKE value. These peak values are located at the very end of the serration tips, making them not visible in Figure 15c. The values along the blade share a similar range around 1 m^2/s^2. The average TKE along the serrations addition is equal to 1.47 m^2/s^2. This is 0.82 m^2/s^2 higher than the average tip value on the basic blade, but is 0.91 m^2/s^2 lower than the average TKE value on the fin addition to the geometry.

4.2.1 Angle of Attack Comparison

Comparing the angle of attack between the results shows that the turbulence intensity right after the turbine is very different. But this varies largely based on the shape. For the serration shape, half a meter behind the blade tip, there are no vortices to be found in the slice taken with a 12 degree AoA, but already strong vortices were present with the blades rotated at 7 degrees. On the other hand, Figure 16 shows that the fin shape had a similar extent of vortices half a meter behind the tip of the blade. Figure 16a shows smaller vortices produced

after the blade is positioned at 7 degrees AoA. This comparison shows that the fin shaped blades also have different points after the blade where the wakes take place depending on the AoA, but not as dramatic an extent as those blades with serrations. The smaller wakes in Figure 16 in this case demonstrate

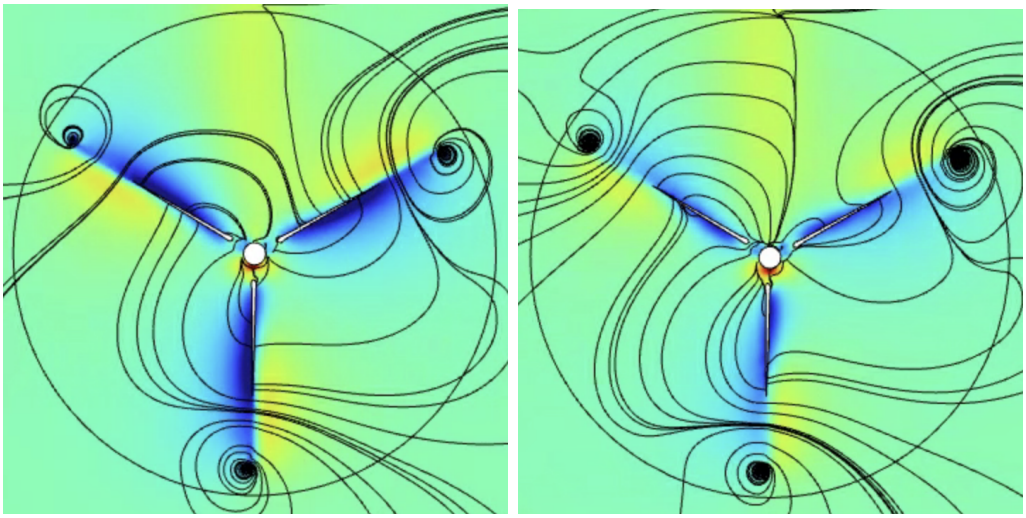

Figure 16: Figure a. 0.5 m behind the fin shape blade with a 7 degree AoA and Figure b. 0.5 m behind the find shape blade with a 12 degree AoA.

In terms of the TKE produced by changing the AoA, there is not a large degree of variation between the three different shapes. This is largely expected due to the fact that there is only a five degree shift between the selections of AoA, but also that the AoA can instead play a larger role for the other relevant metric, namely the power of the turbine based on the lift to drag coefficient. While the AoA's influence by itself only leads to some difference in the position and continued tip vortex intensity, it provides more interesting results in combination with the other tested parameters.

4.2.2 Tripped Blade Comparison

As would be expected with the tripped blade, the average TKE found over the surface of the blades, as well as the supporting structures was higher. In Figure 18, the examples of a tripped blade and a smooth blade are shown with the serrated blade as an example. Something that is immediately noticeable when comparing these results is that the leading edge also has higher identified TKE values. This is easy to attribute to it being the surface with the most interaction with the incoming wind, similar to the supporting features of the turbine. The trailing edge at the center of the blade also has noticeably more intense turbulence as compared to the smooth blade. The geometry at the tip, which in the case of Figure 18 is serrations, also moderately increases in the case of all three blade shapes, but not to the same extent as the leading edge or center trailing edge does.

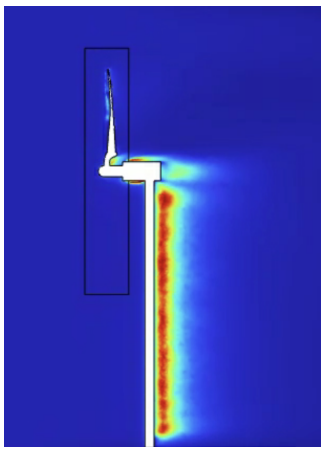

Figure 17: Side profile of a tripped blade (serrations) plotted with TKE. A peak value of $8\frac{m^2}{s^2}$ is shown behind the stem.

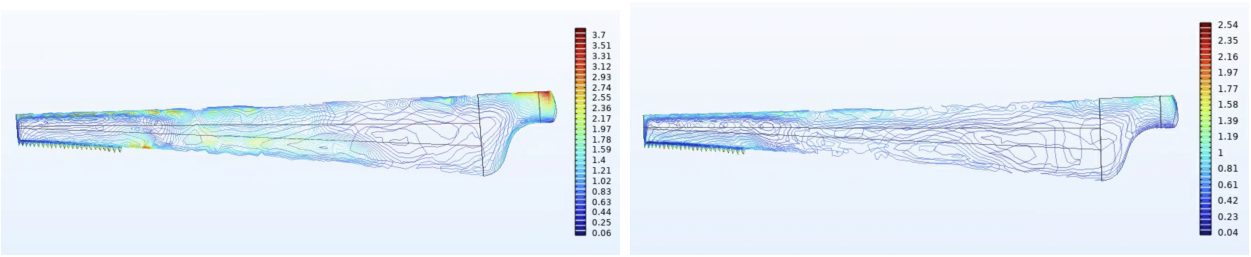

Figure 18: Comparison of the tripped blade (a.) and the smooth blade (b.) for the serrated blade as an example. The TKE is shown, with different ranges for values shown on the right of each image.

The supporting structures such as the central element for mechanical parts and the stem of the turbine contributed significantly more towards the TKE in the case of the tripped blades. Since these structures also counted as walls when defining the boundaries, the roughness of the surfaces contributes much more to their overall turbulence, similar to the way in which the leading edge now produces a larger amount of TKE.

When comparing the effect of tripping the blade at different angles, this was tested on the fin sample with the same five degree difference of 7 against 12 degrees. Unexpectedly, however, the higher degree of rotation showed to have less intensity in the turbulence than the lower AoA. This was reflected in each of the three shapes. Figure 19 shows two blades, the top one with 12 degrees AoA and the lower image with 7 degrees AoA. In this example, there is the same scale for both in terms of TKE. This allows for a fairer comparison, whereby it is clear that along the leading edge of the lower blade (7 degrees AoA) towards the tip of the blade there is more turbulence. This angle is therefore likely to produce more disturbance after the blade in the wakes, which can either be useful or simply be more destructive and create more noise.

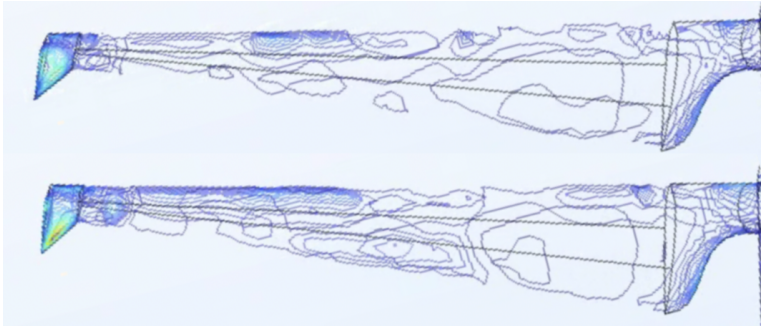

Figure 19: Comparison between tripped blades rotated with a. 12 degree AoA and b. 7 degree AoA.

What is important to conclude from tripping the blade is that the degree to which it influences the noise is not as dramatic as could be expected. It increases the turbulence by approximately 31% at its peak along the leading edge. But whether or not this leading edge noise ultimately makes a difference is still inconclusive. This will be analyzed using MATLAB, as the leading edge noise may not be greater than any of the noise produced by the vortices from the trailing edge. It is important to consider this given that the tripped blade is a more realistic model of wind turbine operation.

4.2.3 Angle of the Wind

The final parameter of interest is the angle of the incoming wind onto the turbine. The measured TKE of this turbine had a much more varied pattern. The TKE of the blade modeled in an upright position has the highest peak value of TKE of $6.35\frac{m^2}{s^2}$ shown in Figure 20a. This value was at the base of the blade as opposed to the tip similar to other results collected. A similar result was observed at the base of one of the other two blades (Figure 20b), where the TKE was highest at the base of the blade.

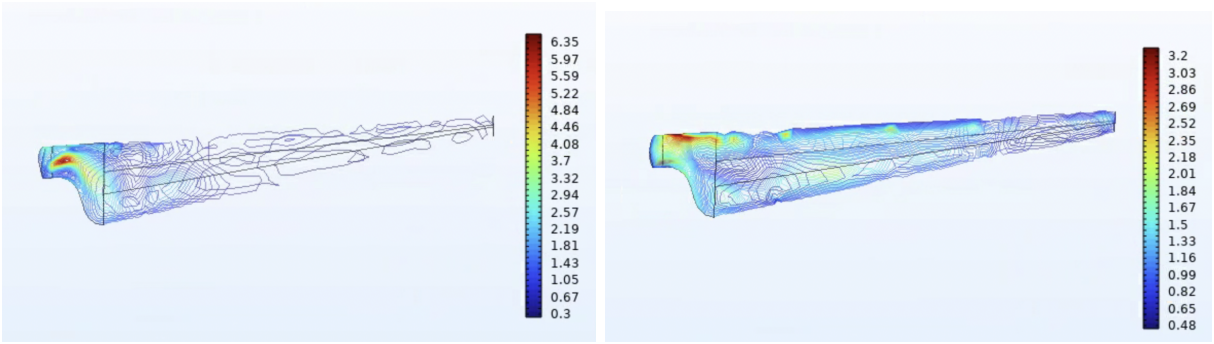

Figure 20: TKE plotted along two blades from the angled wind simulation. Image a. The TKE plotted on the upmost blade of the frozen rotor simulation. Image b. The TKE plotted along the bottom right blade of the frozen rotor simulation.

With the change in direction of the inlet, the flow over the blades does not show any peculiar differences. In Figure 21, the streamlines are shown again. Here, it can be observed similarly to the TKE measurements made that there is a concentration of flow around the base of the blades, surrounding the case with mechanical elements. The flow does have more interaction with this core when the wind approaches from a side angle, hence, it could be expected that more noise would be caused, especially in the case that surface roughness was added. However, this element is stationary, meaning that the flow patterns from the noise would be consistent. From the TKE values and the patterns in streamlines, it can be incurred that these flow settings are interesting to further investigate in terms of noise.

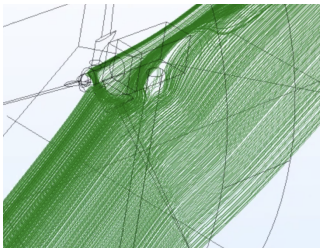

Figure 21: Angled wind velocity patterns over a blade.

4.3 Power of the Turbines

After looking at the TKE patterns of each of the simulations tested, it is also important to look at the larger goal of wind turbines, which remains the production of green energy which can be stored and used by industry and consumers. The metric which can appropriately reflect this in the system is the power of the turbine in Watts. Power can be calculated by integrating the torque produced over the turbine blade surfaces and multiplying it by the angular velocity, as shown in equation 17. This value was calculated in COMSOL for each of the simulations. The corresponding values are shown in Table 2.

$$P = \tau \cdot \omega \tag{17}$$

These values and data cannot be validated within the computational study or otherwise given that they highly vary but do also suit a general range of power which wind turbines fall under. However, one method to test the expected range of values is to calculate the Betz limit. The Betz limit says that no wind turbine can capture more than 16/27 times the maximum kinetic

Table 2: Power outputs calculated from COMSOL per wind turbine simulation run.

Simulations	Basic shape	Blade with fin	Blade with serrations
7 degree AoA, smooth blade	2.57 MW	2.26 MW	1.46 MW
12 degree AoA, smooth blade	2.44 MW	3.53 MW	0.97 MW
7 degree AoA, tripped blade	1.55 MW	1.65 MW	1.72 MW
12 degree AoA, tripped blade	-	2.88 MW	-
7 degree AoA, Right angled wind	3.81 MW	3.72 MW	1.56 MW

energy [46]. This rule of thumb has been used for the past century and is shown in equation 18 [47].

$$P_{\text{Betz}} = \frac{16}{27} \times \frac{1}{2}\rho A V^3 \tag{18}$$

The calculated Betz limit for the simulation turbine is 4.352 MW, which means that any value higher than that is completely unattainable [47]. Already reaching this limit is unrealistic as well. The Betz limit represents the maximum energy that can be converted from kinetic energy. But often the value of this is even lower due to frictional forces and aerodynamic limitations. Approximately 40 to 50% of the Betz limit is seen as a success when it comes to wind turbine design, and 35% is acceptable with larger scale turbines [48]. This means that a range between 1.52 MW and 2.18 MW is expected as realistic. Majority of the simulations were run with smooth blade conditions, which means that these values were, as expected, higher than this realistic range. From the values collected for the tripped blades, the 12 degree angle with the fin blade is the only one which exceeds the Betz limit dramatically.

4.4 MATLAB Data

The MATLAB data is where the flow and pressure values are converted into sound utilizing the SPL theory of equation 14. This can only be analyzed in MATLAB in the 2D domain. The model was validated through testing literature studies and comparing the obtained results. From this validation an error of approximately ±6% was found. The first way in which the data was viewed is with the same cut planes half a meter behind the tip of the blade. The comparison of the blade shapes such as this is shown in Figure 22.

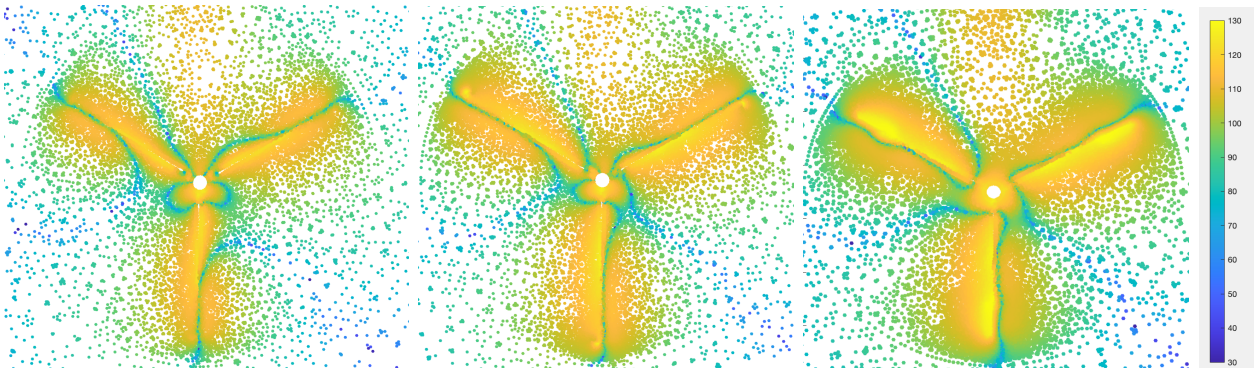

Figure 22: Slice profile 0.5 m behind the tip of the blade measuring the dBA for a. basic shape, b. fin, c. serrations.

This comparison of the slice right behind the tip does not provide much new information. In addition, it varies greatly in terms of precision, as the meshing is much more fine for the

serrated blade, which is why Figure 22c shows a much better resolution. These images have similar insights to the TKE on a specific blade, considering that a slight peak exists on the middle point of the blade, and at the end of the blade there are some increased values depending on the geometry of the blade. Figure 22b for example shows a more intense noise production at every tip of the blade, similarly to what was shown in Figure 15. In terms of values, the area close to the turbine reaches 120 dBA, which can be expected immediately after the blade.

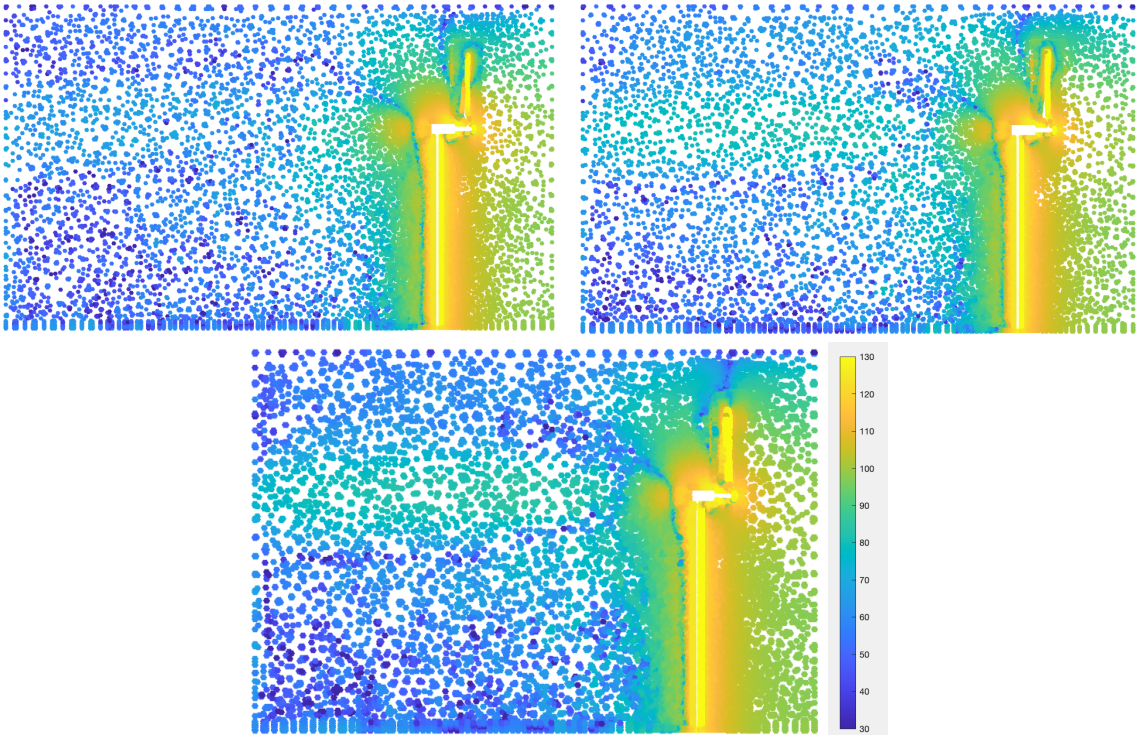

Figure 23: Slice profile capturing the effects behind the turbine, measuring the dBA in the air for a. basic shape, b. fin, c. serrations.

A more useful way to analyze 2D data is by comparing the noise levels behind the turbine. By creating planes on the xz axes, the height and length of the model are visible. In addition, it captures the upmost blade in the frozen rotor results. A comparison between the shapes with the adjusted data measurements is shown in Figure 23.

In Figures 23, there are distinct patterns after the blades in which noise can be observed. The first thing to observe is that, despite having high turbulence and high initial noise, the turbine stem has little influence on the trailing noise after the turbine. Up to a maximum of 50 meters behind the turbine, the stem still shows effects, after which the 40 dB is easily met for each of the three blade shapes. It is also clear that the defined rotatory mesh cylinder of the setup also

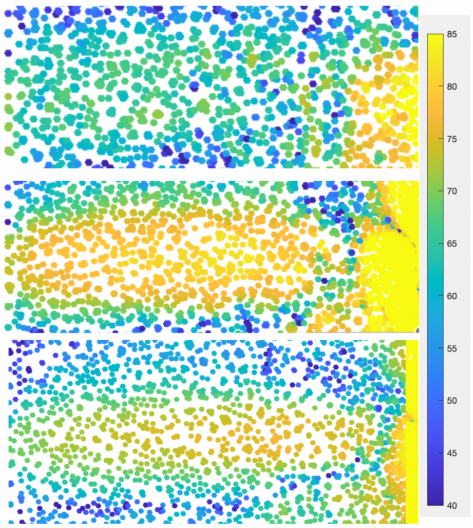

Figure 24: Zoomed in slice showing the air directly behind the turbine radius for a. basic shape, b. fin, c. serrations.

produces some noise. However, what is most interesting about these figures is the clear production of noise which carries over after the turbine blades. This noise was also not identifiable within the COMSOL data, neither when looking at the streamlines nor at the turbulence. A closer look at the air behind the turbines is shown in Figure 24. Between the three shapes, the two that excel are the basic shape and the serrations shape. Which is similar to what was expressed in the COMSOL data, the fin shape is not the preferred shape for noise or turbulence reduction.

All of these can be compared to the base case, which was also implemented in MATLAB to understand the scale of the noise to improve upon and meet the research objective. Figure 25 presents the results of the base case in the same format as the previous samples.

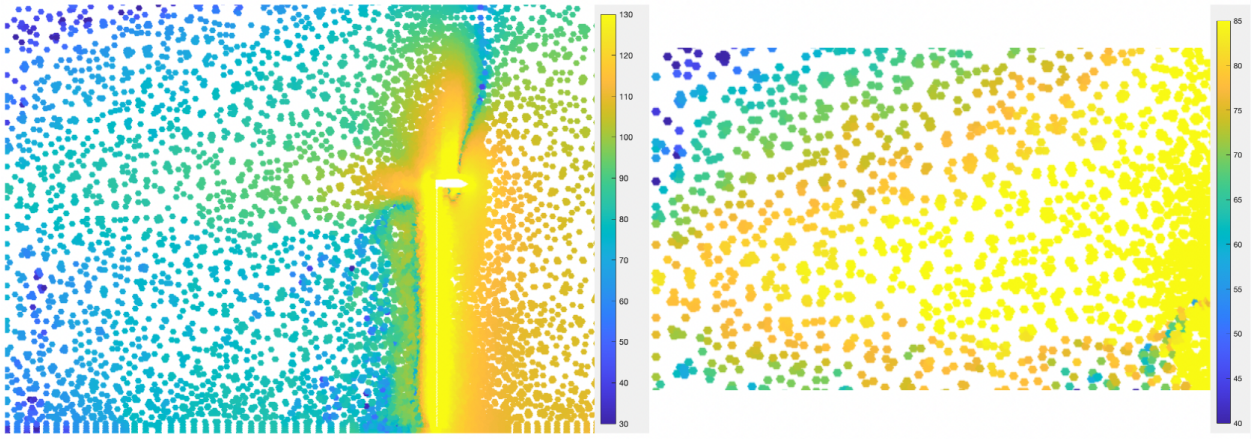

Figure 25: Slice of the base case with a. the full scale of dBA b. zoomed in to behind the blade radius with the adjusted scale of dBA.

The base case shows a similar but more intense noise pattern to the three presented designs. To make a comparison, a noise point directly behind the mechanical case of the turbine, 350 m away at the edge of the data set, was used for each of the four noise tests simulated. The results of this shared that the base case produced a point with 70.38 dBA in value, the basic shape 64.04 dBA, the fin shape 71.40 dBA, and the serrated shape 65.48 dBA. All of these values remain far too high above acceptable values. However, points closer to the ground show more reasonable values. For the base case, 51.82 dBA, the basic shape 46.97 dBA, the fin shape 51.65 dBA, and the serrated shape 48.43 dBA.

4.4.1 Wind Angle Effect on Noise

Based on the results collected in COMSOL, the most positive factor in being able to move the TKE concentration of the blade away from the tip was the wind angle. This factor is more variable than the rugosity or AoA of the blade and showed that it could potentially be useful for producing a less noisy simulation. When tested in MATLAB, each of the results was similar to those collected in COMSOL for rugosity and AoA testing. However, the wind angle was shown to have some variation in the results translating the TKE values into dBA. As shown in Figure 26, there is a higher noise contribution along the entire height of the turbine. Not only does the air behind the turbine directly get influenced in terms of noise, likewise to the patterns shown in Figures 23, but also behind the stem of the turbine there is more noise. This slice is taken in the direction of the inlet wind, similar to those in Figure 22 but rather than perpendicular, now at a 45 degree angle. Behind the turbine gearbox

is the only place in Figure 26 where the noise level drops behind the turbine, for the rest of the air, the noise is shown to be an average of 80 dBA still over the 300 m behind the turbine. Ultimately, while the TKE concentration moved away from the tip in the COMSOL results, the noise did not reflect these same efforts, making the preferred angle of the wind perpendicular to the turbine.

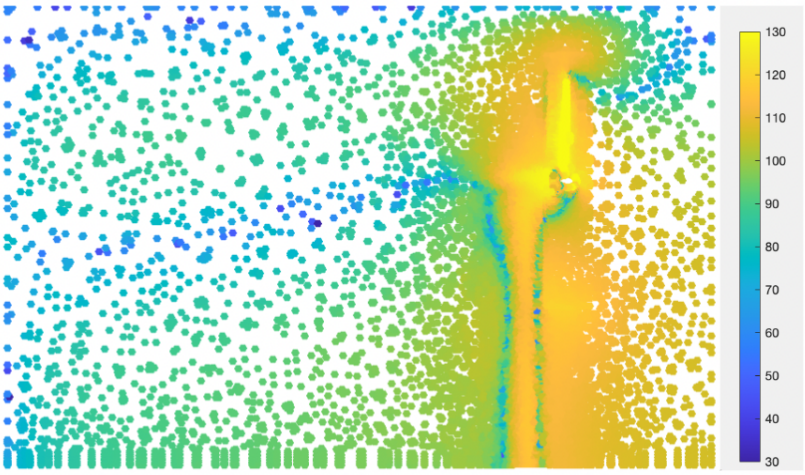

Figure 26: MATLAB results with the wind hitting the blades at a 45 degree angle.

4.4.2 Effect of Blade Rugosity

As expressed by the power produced by the turbines and the wear over use, the blade rugosity is a more accurate way to model real wind turbines. In Figure 27, the same format is once again used to analyze the noise patterns. Given that in Figure 27a, the noise patterns appear to be relatively in line with those presented in Figure 22. However, there is a big difference with the noise directly after the turbine. This is upwards of 90 dBA for up to 75 m behind the turbine, a direct relation to the surface roughness that produces this noise. A further zoom was also made in Figure 27b, where the noise level appears to range between 55 and 70 dBA with the exception of some spots producing upward of 80 dBA. With the same point analysis as done with the other samples, a value of 50.26 dBA is measured. This value is lower than the smooth blade baseline case and is only 1.87 dBA higher than the noise produced by the smooth serrated shape.

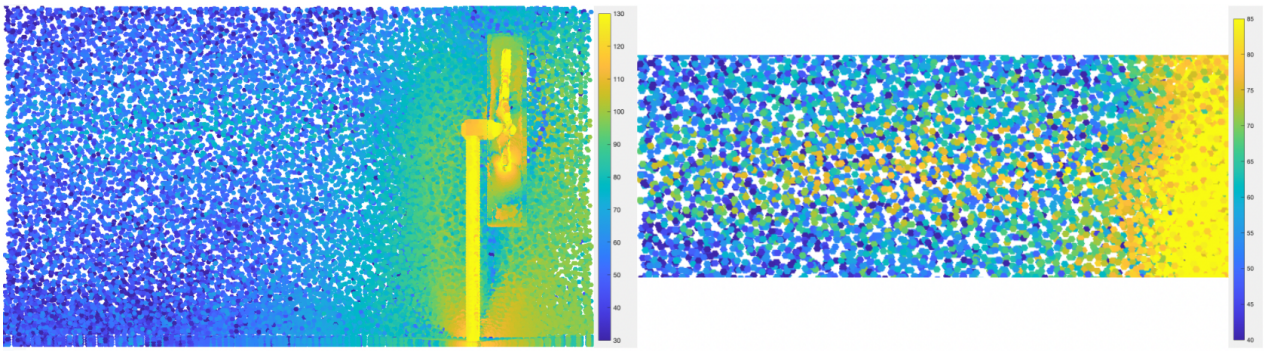

Figure 27: Slice of the tripped rugosity blade (serrations) with a. the full scale of dBA and b. zoomed in to behind the blade radius with the adjusted scale of dBA.

4.4.3 Extended Area Beyond the Turbine

The basic shape and the serration shape with parallel wind both show dBA values between 55 and 75 dB until 300 meters after the turbine, which is where the boundary stops. As a result, these simulations were tested once more with an extended boundary layer, in order to see the extent after which the noise drops to the acceptable level, and whether this is in line with the 450m needed or is shorter. With the boundary layer being pressure controlled, this affects the flow right at the edge meeting this boundary layer. However, the air behind the turbine can be extended in the simulation. This was carried out in COMSOL and exported to MATLAB, shown in Figure 28.

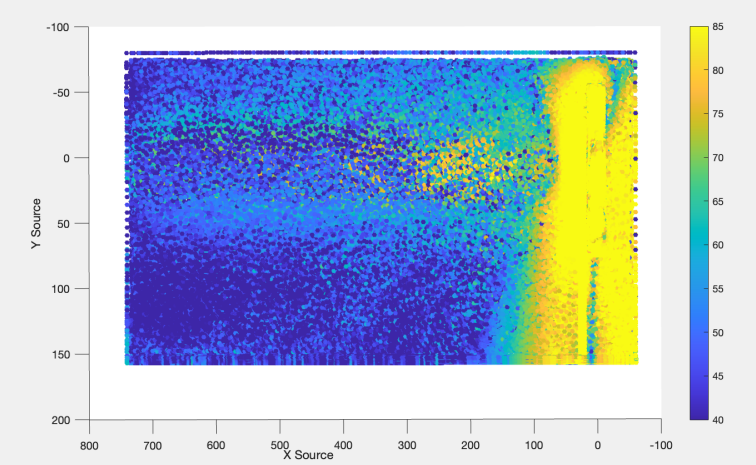

Figure 28: Slice profile with a distance of 800 m behind the turbine for the serrated shape profile, measured in dBA.

A higher definition sound pattern was plotted in Figure 28 for the serrated blade shape. In this image, the intense sound is shown to trail off around 250m behind the turbine. However, some noise continues between 50 and 65 dBA at the highest and lowest part of the blade radius. At the further point from the turbine, the noise is measured to be 38.74 dBA behind the turbine blades. Behind the stem of the turbine, closer to the ground, the noise is measured to be 27.22 dBA.

4.5 Discussion

The results show a clear pattern of improvement with the majority of the data derived from the three different cases presented compared to the base case. The addition of geometric shapes show varying results as to whether or not they improve the acoustic performance of the turbines. In the case of the serrations, this is seen to have an effect on reducing the noise produced, bringing the value down by 3.19 dBA on the ground level. This reduction in noise is mainly attributed to alteration of the airflow characteristics around the blades, which affects the turbulent boundary layer and the mechanisms of sound generation. On the other hand, the blade with a fin shape does not share the same conclusions. The conclusions there show that despite being effective in 2D simulations and singular blade set ups, the rotation of this shape does not successfully disrupt the wake formation in a productive way, leading to a 0.17 dBA noise reduction close to the ground, but an increase of 1.02 dBA in noise at the level of the blades.

One of the key mechanisms which reduces noise is by disrupting the coherent structures

of the turbulent boundary layer along the trailing edge of the blade. Similar research performed found that the implementation of trailing-edge serrations can lead to a reduction in broadband noise levels, particularly at low frequencies [49]. This research also noted a significant reduction in blunt vortex-shedding noise at higher frequencies, demonstrating the effectiveness of serrations in mitigating various noise sources without altering the direction of radiated sound [49]. The frequency was not reflected within the MATLAB model; however, similar findings in terms of noise positively indicate that these results would also be replicated in this study.

In addition, the implementation of serrated trailing edges can enhance the mixing of airflow, which contributes to a more uniform velocity distribution and reduces the correlation length of turbulence at the trailing edge [19]. This increased turbulent mixing diminishes the intensity of the sound generated by the interaction of the TBL with the sharp edges of the blade, thus lowering the overall noise emissions [19]. Similar experiments also found this, showing that serrations can effectively reduce broadband noise by altering the flow behavior around the serration structures [42].

The design of the serrations naturally plays a role in their effectiveness. The geometry of the shapes themselves plays a role in their effectiveness. Especially when maintaining the same aerodynamic efficiency [50]. The goal of the serrations in this study was to be able to find a piece that could be effectively added to existing turbines. The implementation of serrations is a modification that can be retrofitted to existing turbine designs. This adaptability allows for noise reduction without the need for a complete re-design of the turbine [51].

However, a downside to the serration design measured in this research is their influence on aerodynamic efficiency. Although other studies did not share these same findings, in this research the calculations made for the power indicated that the serrated blades was the weakest design in terms of aerodynamic performance. The power output exhibited a lower power output compared to the baseline case, suggesting that further optimization is necessary to balance noise reduction with energy production.

The other main geometry tested in the simulations was the fin addition. The concept of using fins at the tips of wind turbine blades in theory complements the noise reduction achieved through serrations. The fins focus on aerodynamic performance at the tips, which in theory can reduce the intensity of the noise by controlling the flow, and maintain lift performance [52]. However, from the results found in this research, the fin shape was able to maintain a good level of lift, so that the turbine power remained high but the acoustic performance was not up to the standards of the basic and serrated shapes. The only positive this produces is the fact that the geometric addition was still able to maintain high power output does provide hope that the same can be achieved with the serrated design.

Finally, the combination of the shapes as a parameter with the other parameters tested in the simulations needs to be addressed. The AoA was not as interesting alone but provided primarily differences in the power produced, which delivered a performance similar to what was expected with the testing in XFLR5. On the other hand, the rugosity of the blade yielded some different outcomes. This parameter was added to test an additional layer of reality in the simulations, as wear on the turbine blades is expected over time. The addition of this feature to the study reveals that the difference between the TKE of a tripped blade and a smooth blade is not incredibly significant. It did reflect the fact that the wind turbine

stem was ultimately a more important consideration of the study in terms of TKE. This was partially reflected in the noise testing, as the effects on sound were present up to 75 m behind the turbine, but not further. Nevertheless, the effects were not overly concerning in terms of noise produced after 300 m, only increasing by 2 dBA compared to its smooth counterpart and remained lower than the noise produced by the smooth base case. The improved basic shape shared similar results and the fin shape was excluded from testing due to its clear disadvantage in TKE.

Only one value for blade tripping was considered and added to the simulation parameters. This could be improved with more studies to reflect the accumulation over time and will be further reflected on in Chapter 7 of this research. If less roughness is accumulated on the trailing edge, this has the potential to find improvement in the 50.26 dBA currently measured in the noise model.

The final parameter was the wind angle, which had a significant impact on noise production. The noise simulations showed that off axis wind conditions led to greater turbulence intensity behind the turbine radius, as well as below it, unlike any of the other samples. This is unfavorable as it promotes more noise production closer to populations.

In conclusion, the addition of the geometric shapes of fins and serrations to the blades was only effective in the case of the serrations. The fin shape only produced further turbulence which in combination with other parameters yielded unfavorable results. The basic and serrated shape blades showed that with tripped blades, noise reduction from a base case blade is still attainable, but should have the wind primarily incoming from a perpendicular angle. The serration modification is not only effective but also practical, allowing for the retrofitting of existing turbines to meet noise regulations and improve community acceptance. The basic shape, on the other hand, looks more towards the future of blade design.

5 Experimental Results

In order to visualize the computational models in a different manner, experiments were carried out with a flow tank. The use of a flow tank allows for controlled testing, which can then be used to visualize results which yield different insights to only relying on the computational models. This flow tank, or water tunnel, is 40x40 cm in cross section and 1.2 meters in length, shown in Figure 29 and schematically shown in Figure 31. The testing of the three different blade shapes was the key focus with the flow tank; additionally, tests with a different angle and one with a higher velocity were also carried out. The three blade samples were printed to be approximately 25 cm in length, in accordance with the flow tank dimensions. They were printed using a filament 3D printer but with a high degree of precision and on their side to create the smooth surfaces, which are necessary to best visualize the turbulence.

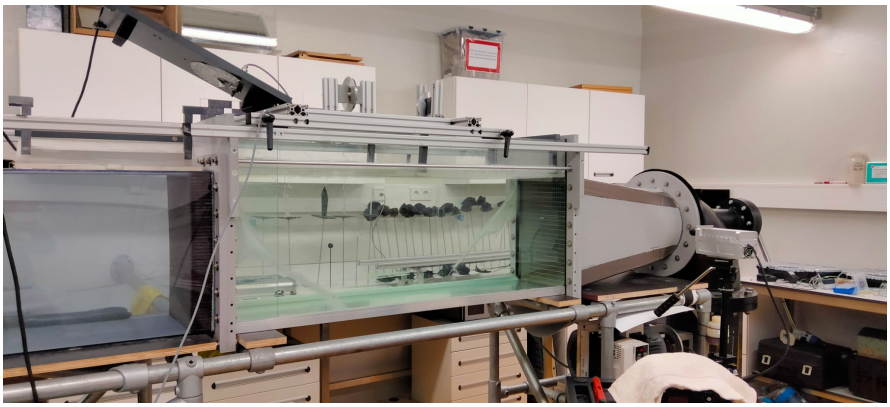

Figure 29: Photograph of the flow tank taken without a sample in it. The cross section is shown in the center of the photo.

The goal of using the flow tank is to be able to visualize the data and use it to draw some different conclusions to the simulation data, while also trying to compare where possible. This will be done with the turbulence, using a method called Particle Image Velocimetry (PIV) to be able to visualize the turbulence and have information on the velocity [53]. This uses the camera and laser setup present in the flow tank to track specific water particles as they travel around the sample. The camera can capture up to 300 frames per second to be able to accurately trace the flow. Further details of the experimental setup will be explained in the following section.

5.1 Experimental Setup

The use of the flow tank is to validate the computational modeling. Therefore, the Reynold's number should match that measured in the computational domain. This is challenging given the use of water, which has a vastly different density and viscosity compared to air. Additionally, the speed of the wind in the simulation is 12 m/s which is accelerated given the centripetal forces at the tip of the blade. The velocity of the water in the tank can operate at an approximate maximum of 1 m/s without causing significant vibrations in the tank. Taking this speed into account, the properties of water along with the Reynold's number computed from the simulations using the properties of air ($6.4 \cdot 10^5$), the length of the sample can be computed.

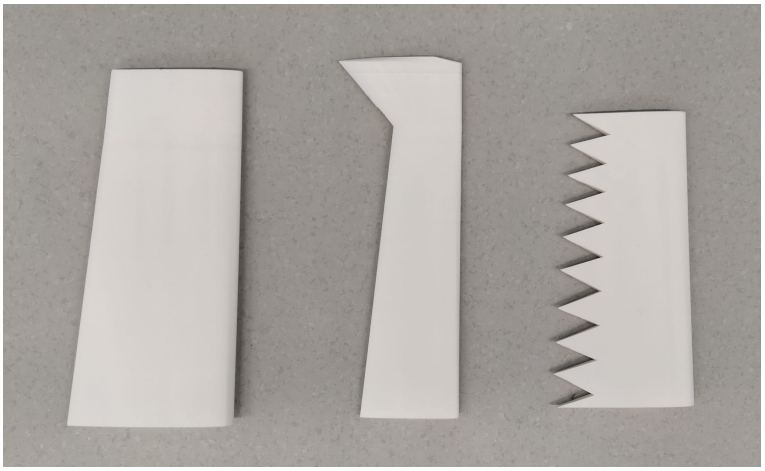

Figure 30: 3D printed samples of the a. basic shape, b. fin shape and c. serrated shape

The most important goal in calculating the necessary length is to be able to reach an order of magnitude of 10^5 in the Reynold's number, to be able to compare with the computational studies. Using the density and viscosity of water and assuming that the flow tank can reach a maximum speed of 1 m/s, the length of the tip must be in the magnitude of 10^{-1}. This is a fairly wide sample, and given the dimensions of the flow tank and the fact that the blade itself has a length:width ratio of 1:0.02, the entire blade was not tested. Instead, only the tip of the blade was printed for testing (samples shown in Figure 30, the width needed being 0.1 m in length, resulting in only printing approximately 10% (depending on the shape) of the blade.

The 3D printed samples, each needed to be supported by a rod in the flow tank to remain stationary during data collection. This support was provided by creating a 5.2 mm diameter hole along the entire blade. This allows the blade to be vertically supported in the tank, as shown in Figure 31. With this, the laser was placed underneath the flow tank in order for the plane of lasers to align with the direction of the flow around the blade. The camera is only able to pick up the flow pattern based on the laser placement. The laser was therefore adjusted to ensure that it was perfectly aligned with the plane to capture the most interesting flow patterns. The camera is placed on the side of this set up, capturing 200 frames per second for PIV.

The data gathered by the flow tank is mainly related to visualization of the flow and extracting some velocity data. As mentioned, the theoretical maximum of the flow tank without vibrations was around 1 m/s; however, maintaining this speed with each of the samples was a challenging task. The stability of the fin shape was a concern due to how thin the printed sample was towards the end of the blade. This meant that the speed of the flow needed to be reduced in order to not move the sample while capturing the pictures, at the expense of reducing the Reynold's number. The flow tank velocity was altered using frequency, with a relation to velocity represented by $v = 0.0189f$. For most data collection, a frequency of 25 $1/s$ was used, which corresponds to a speed of 0.4725 m/s in the tank. This reduced the Reynold's number to the order of magnitude of 10^4.

The most stable and interesting sample for its flow was the serrated shape. With this sample, the support rod (shown between 2 and 4 in Figure 31) was fitted throughout the sample, making it secure. Therefore, a higher velocity of 0.8505 m/s could be tested with this sample. The Reynold number boundary of 10^5 was just missed with this test. Given that the serrated

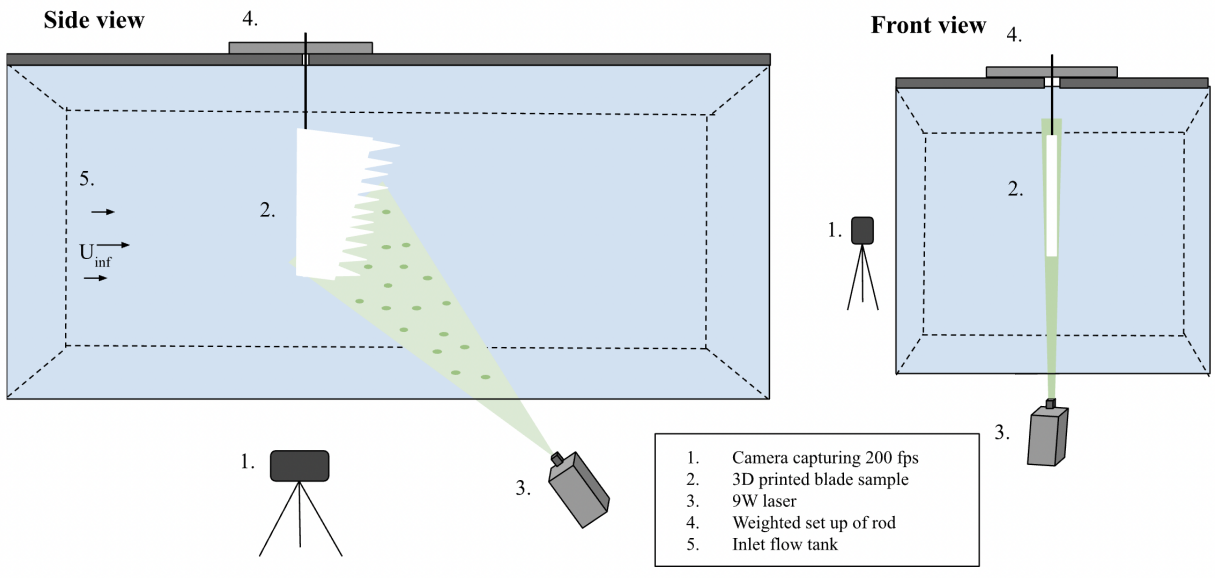

Figure 31: Diagram of the flow tank set up with the serrated blade sample.

blade was also the most interesting profile to test, it was also set at an angle in the tank, which corresponded to an approximated 10 degrees for an additional test. With this test, some conclusions about the AoA could be investigated.

In order to capture all of these results, the camera and laser were needed. The laser was used to set the focus on the particles in the flow tank which could be captured by the camera. The laser utilizes a wavelength of 532 nm, operating with a power of 9W. This high power level was used to achieve more clear pictures of the particles using the camera, which allowed for greater contrast when analyzing the data. After collecting the data with the camera, MATLAB was used once again to interpret this data using PIVlab, an add-on to MATLAB. Ten frames were imported into PIVlab per sample and analyzed for their flow patterns. These frames were analyzed and calibrated by comparing the pixel length to the real length of the samples and the time step between the pictures taken [53]. The location of the sample was also masked in the photo in order to understand exactly where the flow was and to remove any reflection that the camera picked up. After the analysis set up was complete, the information from each of the frames was then extracted as well as a mean frame, which took the mean of each of the vectors to collect more averaged data. These results are then reflected in the following section.

5.2 Experimental Results

The visualization of the data is best shown through the use of streamlines. By drawing a rake of 300 streamlines along each of the mean flow frames, the different samples tested can be compared. All are shown in Figure 32, which first shows the three samples operated parallel to the flow with a velocity of 0.4725 m/s, followed by the high-speed serrated sample and finally the serrated sample at an angle of 10 degrees to the inlet.

The most noticeable patterns in this data show the high-intensity tip vortex. The concentration of streamlines after the tip is mostly visible on the right-hand side of the image. The fin shape shows a split in this tip vortex and the serrated blade samples show some other intense vortices after the serration tips as well. However, it is clear that the tip vortex is

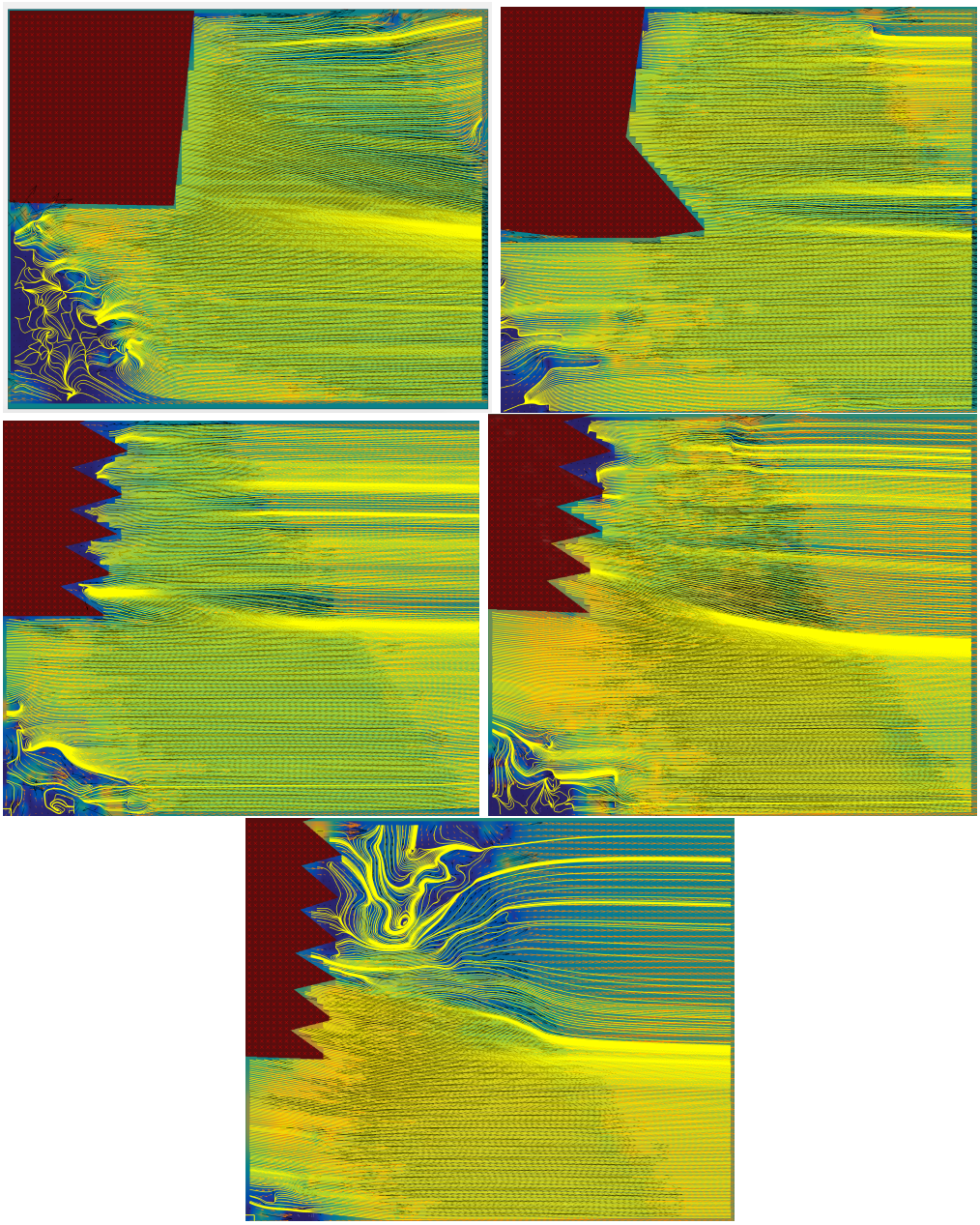

Figure 32: Averaged flow data represented with streamlines. From top to bottom, left to right, The basic shape (a), the fin shape (b) and the serrated shape (c) each operating with frequency set to 25 $1/s$, the serrated shape operating with a frequency of 45 $1/s$ (d). Finally, the serrated shape with a 10 degree angle operating with a frequency set to 25 $1/s$ (e).

most intense in the cases of the serrated blade sample. The high-speed sample and the angled sample show the highest concentration of streamlines after the tip. The visualization demonstrates the presence of these tip vortices, but given that each of the images were calibrated, the velocity of them can also be calculated using PIVlab. These are shown in Table 3.

The values are comparable with the exception of the S45 sample, as this sample had a higher inlet velocity. The tip vortex speed is around 10 times more intense than the inlet flow for each of the other samples. The serrated blade has a higher tip vortex speed compared to the basic or fin shape. The fin shape is fairly low in speed and upon further analysis in PIVlab, it can be reasonably assumed that this data is fairly inaccurate due to it being challenging to see any kind of variation in the data. It appears as though the laser was not positioned

Table 3: The tip vortex velocity measured using PIVlab for each of the experiments.

Sample	**Tip vortex velocity (m/s)**
B25	4.428
F25	3.852
S25	5.141
S45	16.370
S25 angled	5.478

correctly for the collection of its data, presumably making the tip vortex appear smaller, and hence slower. The S45 data, which used the highest inlet velocity, had a tip vortex that is measured to be approximately 20 times faster than the inlet speed. The speeds related to this blade are more closely analyzed in Figure 33.

The serrated blades each have stronger vortices that appear after the serrations. These are clearly shown in the samples that were tested without angles, where there is a clear presence of two additional vortices in the case of the low speed sample, and three in the high speed one. The maximum velocities here only match up to 6 and 11 times the inlet velocity respectively. On the other hand, the angled blade shown in Figure 32e has a significant amount of eddies developed next to the serrations themselves rather than concentrated high speed vortex formation. This intense turbulence presumably leads to the slightly higher tip vortex formulation, but additionally shows some flaws in the use of the serrated design when combined with a higher AoA.

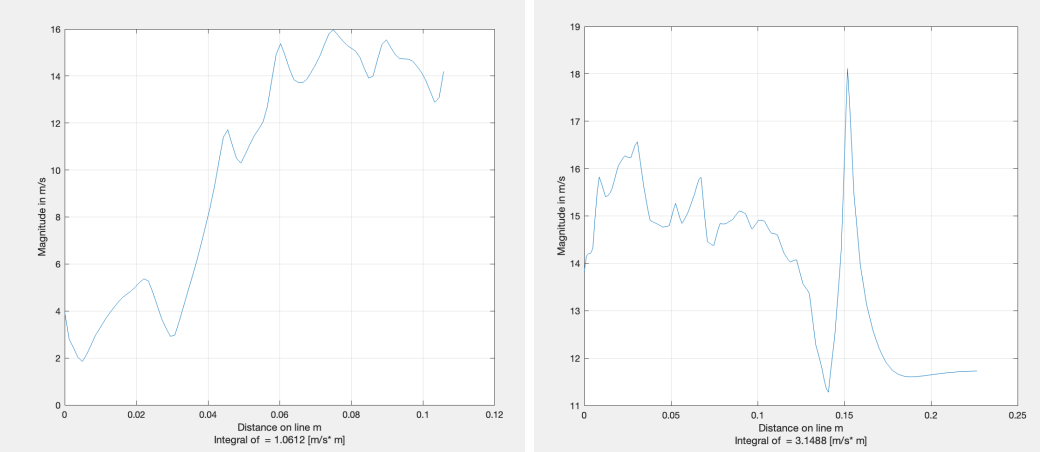

Figure 33: Figure a. The velocity measured along the edge of the sample. Figure b. The velocity measured of the tip vortex.

The left graph of Figure 33 represents the velocity of the flow along the edge of the blade, and the right graph shows the velocity of the tip vortex along the entire image. Both provide more insight into the patterns present in the data collection. The velocity along the edge of the blade increases dramatically when approaching the tip. But it also shows some smaller peaks, correlated to the serrations. The increase in velocity is shown for the last four serrations. This indicates that these already influence the tip vortex. In the right graph of Figure 33, the velocity of the tip vortex slows with the exception of 0.15m where a high peak is present. This is likely a random vector that is caught in the line. Nevertheless, these results show a quick deterioration in speed 0.1m behind the blade.

The final important thing to address is the turbulence underneath the samples. This turbulence occurs differently per sample, with very intense disruptions present for the basic case. Some presence of eddies is also shown in each of the other samples, with the least present in the angled case, where only a small amount of flow disruption is shown at the very bottom of the frame. This can probably be attributed to the bottom of the flow tank. The basic sample was the longest sample created and hence had the shortest distance to the bottom of the tank, likely creating the much more intense turbulence pattern than the other four frames. The angled sample shows that the camera was placed higher as an extra serration is present in the frame compared to the non-angled serration tests. The other three frames show a similar amount of turbulence under the sample.

5.3 Improvements to the Design

The purpose of using the flow tank was to primarily gain insight by visualizing the flow using a different method than computationally. The most interesting way to compare the flow tank results with the computational results is to look at the speed of the vortex produced by the tip.

Looking at the tip vortex velocity of each of the samples, an interesting design improvement can be introduced. The tip vortex was shown to be significantly strong with each of the three shapes and by far the quickest compared to any vortices detected along the side of the blade. The serrations shapes had the quickest tip vortices, and since this shape showed the most evidence of being useful in the computational designs, this combination of factors is something to address. The shape would have more potential if the tip vortex was not as strong, because this is a smaller force creating noise [19]. This could be achieved by ending the placement of the serrations earlier on the blade in order to not interfere with the tip vortex being created already by the blade simply ending. Therefore, if the serrations ended earlier along the blade, then similar results could be achieved along the majority of the trailing edge, while not interacting with the very edge of the blade.

In order to test whether this design could have more potential than the current proposed design of serrations which was tested in COMSOL, the three final serrations were removed from the computational model, and the results were simulated again. The COMSOL results in Figure 34 reflect the intensity of the tip vortex 0.5 m behind the original serrated design and the new serrated design. The tip vortices are more focused in Figure 34b which is shown by less streamlines leaving the blade. Nevertheless, the tip vortices remain intense, even appearing stronger in speed in the case of the top left blade of Figure 34.

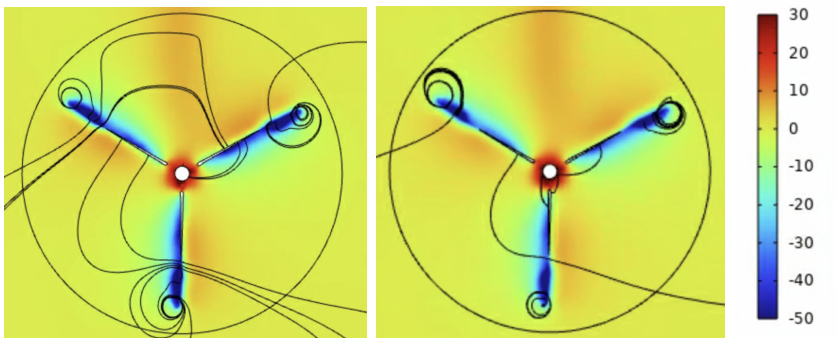

Figure 34: Streamlines and Pressure plotted 0.5 m behind the blade tips of a. Original serrated design b. New serrated design

In order to see whether this is reflected in noise as well as just in tip vortex speed, the MATLAB code was reintroduced. In Figure 35 both the original and new serrated design are compared side by side once more, only looking at the flow patterns behind them. These two appear very similar, but nevertheless have some variation between them. The last sound measurement made at the edge of the image is 65.48 dBA for the original design, versus 63.68 dBA for the altered design. Slight differences in colors can also be seen directly underneath the blade area in favor of the new serrated design.

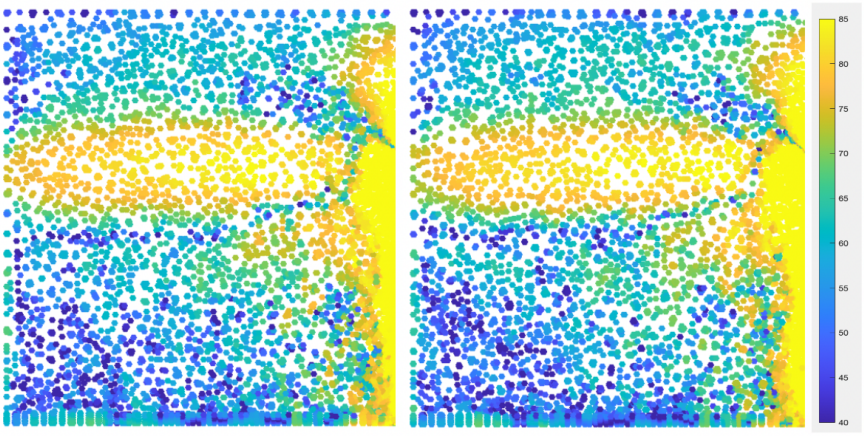

Figure 35: dBA patterns behind the turbine for a. Original serrated design b. New serrated design

These outcomes are positive for incrementally improving the serrated blade design, ultimately resulting in a 6.70 dBA reduction compared to the base case. In addition to offering a 1.80 dBA reduction from the original serrated blade design. Closer to the ground, these values become a 0.65 dBA improvement to the serrated design and a 3.84 dBA improvement to the base design.

6 Conclusion

This study explored the aerodynamic noise reduction of wind turbine blades through CFD simulations and use of a flow tank to further refine the designs. The focus was placed on the formulation of turbulence in order to measure and test varying designs. The designs investigated the parameters of blade geometry, AoA, wind angle and blade rugosity, with attention falling primarily on the blade shape. The results demonstrate that serrated trailing edges significantly reduce noise by disrupting turbulent structures. Serrated blades reduced peak noise by 6.7 dBA and noise closer to the ground by 3.84 dBA with a corresponding 9.8% decrease in TKE. The dBA was further reduced by introducing a design improvement of reducing the number of serrations next to the tip of the blade. However, a trade-off was observed as the power output decreased by 4.2%. The basic shape, which flattened the blade, also experienced similar scale results, also achieving the 3 dBA reduction benchmark. This indicated that two of the shapes, with some variety in other parameters were able to obtain the 3 dBA objective set for the research. In contrast, fin-based designs, while promising in 2D analyses, were less effective in the full turbine setup due to unfavorable vortex formations. The impact of blade rugosity showed as predicted an unfavorable relation with noise formation. Changing the wind angle on the other hand showed moderate TKE formation, but with higher concentrations towards the base of the blades, ultimately however, this did not reflect well for the noise formation with a tilt in the angle, making a perpendicular angle favorable. The AoA was found to only make impact when combined with other parameters. The testing of the combination of the different parameters contributed to novel understanding of approaching noise reduction.

Although noise reduction must still be balanced with turbine efficiency, this study highlights the potential for optimized blade modifications that were able to achieve a 3 dBA reduction with the potential to still be able to meet expected power requirements. A 3 dBA sound reduction is barely noticeable to the human ear, but plays a large role in the requirements and the long term effects of being exposed to loud sounds.

7 Future Work

The first way to improve and develop the models made for this research is to change from a frozen-rotor approach to a time-dependent study. A time-dependent study will reintroduce all of the terms of the SST equations as well as the terms part of the FW-H equation that were transient. While these terms are smaller in contribution to the source of noise than those that are position based, they remain relevant for developing a fully accurate model. In addition, time-dependent simulations offer better tracing of turbulence and a better understanding of the formation of such activity. With short time steps, specific streamlines can be traced and analyzed to understand their vortex patterns. This can better analyze the influence of geometric additions to the blades. With longer time steps, the major sound effects can better be understood and accounted for with the transient terms of SST and FW-H.

Another way to improve the models themselves also relates back to the aforementioned design steps. As described in Chapter 3, LES is regarded as a higher quality CFD model than RANS. It is better at capturing turbulence due to it resolving large turbulent eddies, making it better for dynamic flows. RANS averages out all the turbulence, which does not make it inaccurate, but it can be improved by using LES instead.

LES can also be combined with an acoustic analysis within COMSOL. Other simulation softwares can alternatively be used for performing the CFD analysis, which are FVM based. But, in order to obtain the best resolution of turbulence, COMSOL utilizing LES will be perfectly sufficient. Using a multiphysics coupling system in COMSOL will also better reflect the dBA delivered specifically by turbulence, providing more accurate results.

Finally, one of the best ways to develop a more accurate and realistic model is to improve the modeling of the blade rugosity. The current model utilized $k-\epsilon$ given that an even surface roughness was applied across the turbine. Although applying a roughness parameter to the model is a more realistic way of simulating the turbine in comparison to smooth blades, the equal distribution rugosity on the blade is inaccurate, as over time there would be much more accumulation along the leading edge of the blade and other surfaces which directly face the incoming wind versus those which do not. In the results of this study, it was clear that the leading edge and other surfaces making direct contact with the wind ultimately did play a larger role in the surface turbulence, hence a better model is needed to increase the rugosity on these surfaces or to at least establish some difference between the varying surfaces involved in the simulations.

One way in which this can be studied using CFD is by particle tracing. By following specific particles mixed with the incoming air, the patterns of accumulation along the entire blade can be better modeled in accordance with the turbulence parameters. This method is also more suitable for SST or $k-\omega$ models which is better for the quality of the results, especially along the studied surfaces. Being able to further analyze the rugosity in different methods would lead to deeper understanding of the realistic conditions, which can subsequently be used in researching how coatings may be able to help in terms of noise reduction.

References

[1] Rijksoverheid, "Windenergie op land," 2024, accessed: 2024-10-03. [Online]. Available: https://www.rijksoverheid.nl/onderwerpen/duurzame-energie/windenergie-op-land#:~:text=Nederland%20heeft%20via%20het%20Klimaatakkoord,ondernemers%20en%20organisaties%20of%20omwonenden.

[2] CBS, "Wind turbines in the netherlands," 2022, accessed: 2024-10-03. [Online]. Available: https://longreads.cbs.nl/the-netherlands-in-numbers-2022/how-many-wind-turbines-in-the-netherlands/

[3] Vestas, "Energy payback," 2024, accessed: 2024-10-08. [Online]. Available: https://www.vestas.com/en/sustainability/environment/energy-payback

[4] U.S. Environmental Protection Agency (EPA), "Wind turbines fact sheet," 2019, accessed: 2024-10-08. [Online]. Available: https://www.epa.gov/sites/default/files/2019-08/documents/wind_turbines_fact_sheet_p100il8k.pdf

[5] C. Hansen and K. Hansen, "Recent advances in wind turbine noise research," in *Acoustics*, vol. 2, no. 1. MDPI, 2020, p. 13.

[6] A. L. Rogers and J. F. Manwell, "Wind turbine noise issues," *White paper by Renewable Energy Research Laboratory, University of Massachusetts at Amherst, Amherst, MA*, 2004.

[7] V. Katinas, M. Marčiukaitis, and M. Tamašauskienė, "Analysis of the wind turbine noise emissions and impact on the environment," *Renewable and Sustainable Energy Reviews*, vol. 58, pp. 825–831, 2016.

[8] S. Oerlemans, "Siemens seminar on aeroacoustics: Wind turbine noise," 2021, accessed: 2024-11-01. [Online]. Available: https://www.youtube.com/watch?v=MXwaApwP9iM

[9] J. K. Kirkegaard, T. H. Cronin, S. Nyborg, and D. N. Frantzen, "The multiple understandings of wind turbine noise: Reviewing scientific attempts at handling uncertainty," *Wind Energy Science Discussions*, vol. 2024, pp. 1–32, 2024.

[10] R. J. Stevens, D. F. Gayme, and C. Meneveau, "Effects of turbine spacing on the power output of extended wind-farms," *Wind Energy*, vol. 19, no. 2, pp. 359–370, 2016.

[11] L. D. Knopper and C. A. Ollson, "Health effects and wind turbines: A review of the literature," *Environmental health*, vol. 10, pp. 1–10, 2011.

[12] NS Energy, "Challenges faced by installation vessels amid growing offshore wind turbines," 2023, accessed: 2024-10-27. [Online]. Available: https://www.nsenergybusiness.com/analysis/challenges-faced-by-installation-vessels-amid-growing-offshore-wind-turbines

[13] S. A. Stansfeld and M. P. Matheson, "Noise pollution: non-auditory effects on health," *British medical bulletin*, vol. 68, no. 1, pp. 243–257, 2003.

[14] U.S. Department of Energy. (2024) Wind turbine sound and health effects. Accessed: 2024-10-03. [Online]. Available: https://windexchange.energy.gov/projects/sound#:~:text=On%20average%2C%20land%2Dbased%2C,to%20a%20home%20or%20building

[15] DutchNews.nl. (2015) Dutch wind turbines too close to homes. Accessed: 2024-10-01. [Online]. Available: https://www.dutchnews.nl/2015/09/dutch-wind-turbines-too-close-to-homes/#:~:text=The%20research%20was%20carried%20out,and%20in%20Denmark%201%2C050%20metres

[16] German Wind Energy Association (BWE), "Regulatory distance rules for wind turbines above 2 mw," 2021, accessed: 2024-12-04. [Online]. Available: https://www.wind-energie.de

[17] M. L. Shaltout, Z. Yan, D. Palejiya, and D. Chen, "Tradeoff analysis of energy harvesting and noise emission for distributed wind turbines," *Sustainable Energy Technologies and Assessments*, vol. 10, pp. 12–21, 2015.

[18] C. M. Nyborg, A. Fischer, P.-E. Réthoré, and J. Feng, "Optimization of wind farm operation with a noise constraint," *Wind Energy Science Discussions*, vol. 2022, pp. 1–34, 2022.

[19] W. Liu, "A review on wind turbine noise mechanism and de-noising techniques," *Renewable Energy*, vol. 108, pp. 311–320, 2017.

[20] M. Ye, H.-C. Chen, and A. Koop, "Verification and validation of cfd simulations of the ntnu bt1 wind turbine," *Journal of Wind Engineering and Industrial Aerodynamics*, vol. 234, p. 105336, 2023.

[21] H. Van den Akker and R. F. Mudde, *Transport Phenomena: The Art of Balancing*. Delft: Delft Academic Press / VSSD, 2014.

[22] C. J. Doolan, D. J. Moreau, and L. A. Brooks, "Wind turbine noise mechanisms and some concepts for its control." *Acoustics Australia*, vol. 40, no. 1, 2012.

[23] E.-R. A. University, "Introduction to boundary layers," 2022, accessed: 2024-10-27. [Online]. Available: https://eaglepubs.erau.edu/introductiontoaerospaceflightvehicles/chapter/introduction-to-boundary-layers/

[24] B. J. Cantwell, "The naca airfoil series," 2024, accessed: 2024-10-27. [Online]. Available: https://web.stanford.edu/~cantwell/AA200_Course_Material/The%20NACA%20airfoil%20series.pdf

[25] S. Oerlemans, P. Sijtsma, and B. M. López, "Location and quantification of noise sources on a wind turbine," *Journal of sound and vibration*, vol. 299, no. 4-5, pp. 869–883, 2007.

[26] Z. Xu, J. Wei, S. Zhang, Z. Liu, X. Chen, Q. Yan, and J. Guo, "A state-of-the-art review of the vibration and noise of wind turbine drivetrains," *Sustainable Energy Technologies and Assessments*, vol. 48, p. 101629, 2021.

[27] A. Bodling, B. R. Agrawal, A. Sharma, I. Clark, W. N. Alexander, and W. J. Devenport, "Numerical investigations of bio-inspired blade designs to reduce broadband noise in aircraft engines and wind turbines," in *55th AIAA Aerospace Sciences Meeting*, 2017, p. 0458.

[28] M. F. Barone, "Survey of techniques for reduction of wind turbine blade trailing edge noise." *Office of Scientific and Technical Information*, 2011.

[29] C. Soraghan, W. Leithead, and P. Jamieson, "Influence of lift to drag ratio on optimal aerodynamic performance of straight blade vertical axis wind turbines," *EWEA Annual Wind Energy Event 2013*, 2013.

[30] J. D. Anderson, *Computational Fluid Dynamics: The Basics with Applications*. New York: McGraw-Hill, 1995.

[31] S. Bilbao, "Modeling of complex geometries and boundary conditions in finite difference/finite volume time domain room acoustics simulation," *IEEE Transactions on Audio, Speech, and Language Processing*, vol. 21, no. 7, pp. 1524–1533, 2013.

[32] F. Molina-Aiz, H. Fatnassi, T. Boulard, J.-C. Roy, and D. Valera, "Comparison of finite element and finite volume methods for simulation of natural ventilation in greenhouses," *Computers and electronics in agriculture*, vol. 72, no. 2, pp. 69–86, 2010.

[33] COMSOL, "The finite element method (fem)," 2017, accessed: 2025-01-10. [Online]. Available: https://www.comsol.com/multiphysics/finite-element-method

[34] J. E. F. Williams and D. L. Hawkings, "Sound generation by turbulence and surfaces in arbitrary motion," *Philosophical Transactions of the Royal Society A: Mathematical, Physical and Engineering Sciences*, vol. 264, no. 1151, pp. 321–342, 1969.

[35] S. Bouterra, R. Belamadi, A. Djemili, and A. Ilinca, "Flow separation control and aeroacoustic effects of a leading-edge slat over a wind turbine blade," *Energies*, vol. 17, no. 22, p. 5597, 2024.

[36] A. L. Rogers, J. F. Manwell, and S. Wright, "Wind turbine acoustic noise," *Renewable Energy Research Laboratory, Amherst: University of Massachusetts*, 2006.

[37] G. van Kuik and W. Bierbooms, "Introduction to wind turbine design," *Eindhoven: Delft University Wind Energy Research Institute*, p. 16, 2002.

[38] P. Richards and S. Norris, "Appropriate boundary conditions for computational wind engineering models revisited," *Journal of Wind Engineering and Industrial Aerodynamics*, vol. 99, no. 4, pp. 257–266, 2011.

[39] B. Y. Kassa, A. T. Baheta, and A. Beyene, "Aerodynamic performance characteristics of low re airfoils: A parametric and multi criteria decision study," *Results in Engineering*, vol. 24, p. 103174, 2024.

[40] M. A. El Hady, "A comparative study for different shapes of airfoils," *Journal of Advanced Research in Fluid Mechanics and Thermal Sciences*, vol. 69, no. 1, pp. 34–45, 2020.

[41] S. Seevers, R. Ward, S. Hutto, D. House, N. Zelenka, M. Perea, and D. Fonseca, "Wind turbine noise reduction through blade retrofitting," *Open Journal of Modelling and Simulation*, vol. 12, no. 3, pp. 75–88, 2024.

[42] Z. Ning, R. Wlezien, and H. Hu, "An experimental study on small uav propellers with serrated trailing edges," 2017.

[43] E. Sagol, M. Reggio, and A. Ilinca, "Issues concerning roughness on wind turbine blades," *Renewable and sustainable energy Reviews*, vol. 23, pp. 514–525, 2013.

[44] K. Meister, T. Lutz, and E. Krämer, "Development of a process chain for a detailed wake simulation of horizontal axis wind turbines," *EUROMECH [508]-Wind turbine wakes, Madrid*, 2009.

[45] C. Masson, C. Sibuet-Watters, S.-P. Breton, and J. Sumner, "Use of actuator disk and actuator surface methods for the aerodynamic modeling of wind turbines: A review," *Wind Turbine Wakes*, p. 32, 2009.

[46] A. Betz, *Introduction to the Theory of Flow Machines*. Pergamon Press, 1966.

[47] A. Rauh and W. Seelert, "The betz optimum efficiency for windmills," *Applied Energy*, vol. 17, no. 1, pp. 15–23, 1984.

[48] J. F. Manwell, J. G. McGowan, and A. L. Rogers, *Wind energy explained: theory, design and application*. John Wiley & Sons, 2010.

[49] E. Llorente and D. Ragni, "Trailing edge serrations effects on the aerodynamic performance of a naca 643418," *Wind Energy*, vol. 22, no. 3, pp. 392–406, 2018.

[50] B. Song, L. Xu, K. Zhang, and J. Cai, "Numerical study of trailing-edge noise reduction mechanism of wind turbine with a novel trailing-edge serration," *Physica Scripta*, vol. 98, no. 6, p. 065209, 2023.

[51] K. Qaissi, O. Elsayed, M. Faqir, and E. Essadiqi, "Aerodynamic optimization of trailing-edge-serrations for a wind turbine blade using taguchi modified additive model," *Energies*, vol. 16, no. 3, p. 1099, 2023.

[52] C. León, R. Martinez, S. Pröbsting, D. Ragni, and F. Avallone, "Acoustic emissions of semi-permeable trailing edge serrations," *Acoustics Australia*, vol. 46, no. 1, pp. 111–117, 2017.

[53] W. Thielicke, "Pivlab - particle image velocimetry (piv) tool with gui," 2023, accessed: 2025-03-05. [Online]. Available: https://nl.mathworks.com/matlabcentral/fileexchange/27659-pivlab-particle-image-velocimetry-piv-tool-with-gui